GEAP-10236
AEC Research and
Development Report
October 1970

FAILURE BEHAVIOR OF FLAWED CARBON STEEL PIPES AND FITTINGS

M. B. Reynolds

Approved: S. R. Vandenberg
S. R. Vandenberg
Project Engineer

Approved: D. H. Imhoff, Manager
D. H. Imhoff, Manager
Development Engineering

Prepared for the
U. S. Atomic Energy Commission
Contract AT(04-3)-189
Project Agreement 37

ATOMIC POWER EQUIPMENT DEPARTMENT • GENERAL ELECTRIC COMPANY
SAN JOSE, CALIFORNIA 95125

6169-Dev. Eng.-XXX
250-MS-10/70

GENERAL ELECTRIC

DISCLAIMER

NOTICE

GEAP-10236
AEC Research and
Development Report
October 1970

FAILURE BEHAVIOR OF FLAWED CARBON STEEL PIPES AND FITTINGS

M. B. Reynolds

Approved: S. R. Vandenberg
S. R. Vandenberg
Project Engineer

Approved: D. H. Imhoff
D. H. Imhoff, Manager
Development Engineering

Prepared for the
U. S. Atomic Energy Commission
Contract AT(04-3)-189
Project Agreement 37

ATOMIC POWER EQUIPMENT DEPARTMENT ● GENERAL ELECTRIC COMPANY
SAN JOSE, CALIFORNIA 95125

6169-Dev. Eng.-XXX
250-MS-10/70

GENERAL ELECTRIC

NOTICE

TABLE OF CONTENTS

LIST OF ILLUSTRATIONS

LIST OF TABLES

ABSTRACT

The pressure load limit for a cylindrical shell containing a flaw is a function of cylinder radius and wall thickness, flaw dimensions, and properties of the material. The strength of large diameter thin-wall cylinders of brittle material containing axial through-wall flaws can be predicted by linear elastic fracture mechanics if corrections for effect of curvature are made. Expressions to predict pressure load limits in more ductile materials become more empirical. Such expressions have been developed by several investigators.

Pressure load limits for cylinders containing full-length, axial, part-through flaws can be predicted by equating the effective stress in the ligament at the base of the flaw to the plastic instability stress for the material. Load limits for cylinders having short part-through flaws are predicted from a failure diagram in which relative burst pressure is plotted against the reciprocal of flaw length.

Results of hydrostatic tests at 60°F on flawed ASTM A106B pipes in nominal diameters ranging from 4 to 12 inches are presented. Results of tests on pipes with axial through-wall flaws are compared with empirical equations. Results of burst tests on flawed tees and elbows are presented.

1. INTRODUCTION

The objective of the Reactor Primary Coolant System Rupture Study is to determine the modes by which reactor piping might fail, the processes leading up to the failure, and finally the numerical probability that such a failure might occur. Two distinct kinds of failures must be recognized: (1) a leak resulting from a crack or other flaw in the wall of a pipe or fitting, and (2) a sudden fracture failure under monotonic load as a result of a flaw in a pipe or fitting. The mechanism by which a flaw is produced in a pipe or fitting is outside the scope of this report; it shall deal only with the failure of flawed structures under monotonic load and the relationship between failure load and flaw size.

The presence of a flaw in any stressed structure, such as a pipe, may be expected to reduce the maximum load which it can support. The design load for an unflawed structure is commonly well below the value at which general yielding would occur. A large enough flaw in any structure can cause a failure at a below-yield load by virtue of simple loss of load-bearing cross section; how large a flaw is required depends on the shape of the flaw and the deformation properties of the material. If the material is brittle, a relatively low load may be enough to bring the local stress at the tip of a sharp flaw to the fracture level and cause the structure to fail as a result of unstable fracture propagation. If the flaw configuration is geometrically simple enough that the elastic stress field about its tip can be determined theoretically or experimentally, the gross stress at which failure will occur can be estimated in terms of a single material constant. This constant is the "plane strain fracture toughness", K_{Ic}, of linear elastic fracture mechanics. Within the range of applicability of linear elastic fracture mechanics, the gross failure stress is almost entirely dependent on material properties, flaw size and flaw configuration, and is but slightly dependent on the size of the structure.

If a sharp flaw exists in a ductile material, an increasing load causes plastic deformation to occur first in the region of the highest local stress at the tip of the flaw. Deformation tends to reduce the acuity of the flaw tip and consequently the local stress concentration. Hence, a larger flaw is required to produce a failure at a given stress level in a ductile material than in a brittle one.

For brittle materials, the mathematics of linear elastic fracture mechanics predict that the product of flaw diameter or length and the square of applied stress at fracture should be a constant. This prediction has been experimentally verified for simple flaw configurations such as a semi-elliptical surface crack in a large plate under tension normal to the crack plane, an edge crack in a plate under tension, or a through-wall crack in a plate under tension. If the material is somewhat ductile (but not so ductile that plastic deformation extends very far from the flaw tip before failure occurs), the fracture failure stress can still be estimated by correcting the macroscopic flaw length by an amount comparable to the size of the plastic zone at the flaw tip. Since this correction is a function of the ratio of the fracture toughness of the material to its yield stress, another material constant has been introduced into the estimation of the failure stress and some of the simplicity of linear elastic

fracture mechanics is lost. The technique is useful, however, for dealing with ductile materials in sections of thickness exceeding the size of the plastic zone. For ductile materials in thin sections, linear elastic fracture mechanics is of limited value in predicting failure stresses under monotonic loading, and empirical techniques must be used.

2. GENERAL TESTING PLAN

In the following paragraphs, some experiments on the failure behavior of ASTM A106B steel pipes and fittings containing different kinds of flaws are discussed. The use of empirical equations to predict failure pressures of flawed pipes is also considered.

2.1 PIPES WITH LONG AXIAL PART-THROUGH CRACKS

A pipe containing a long (several pipe diameters) axial part-through flaw of constant depth may be considered analogous to a series-connected pair of cylindrical tensile elements. In this analogy, the ligament remaining at the base of the flaw would be represented by the smaller, plastically deforming member of the pair; the unflawed portion of the pipe would be represented by the larger, elastically loaded element. The load maximum for a two-element structure of this kind coincides with the onset of plastic instability in the smaller of the two elements. This coincidence suggests that a pipe containing a long part-through flaw should fail when plastic instability occurs in the ligament at the base of the flaw.

To apply this hypothesis to a pipe containing a long part-through flaw, it is necessary to estimate the three principal stresses effective in the ligament at the base of the flaw and the plastic instability stress for the material under triaxial stress conditions. By denoting axial, circumferential, and radial stresses in a pipe under internal pressure by σ_1, σ_2, and σ_3, respectively, the average principal stresses in the ligament can be approximated in terms of the applied nominal hoop stress σ_h:

$$\sigma_1 = \sigma_h/2, \tag{1a}$$

$$\sigma_2 = \frac{T}{x}\,\sigma_h, \tag{1b}$$

and

$$\sigma_3 \simeq \frac{\nu}{2}\,(\sigma_1 + \sigma_2) \tag{1c}$$

where:

T = unflawed wall thickness,
x = thickness of the ligament,
ν = elastic Poisson ratio for the material.

The ratio of the nominal hoop stress based on unflawed pipe dimensions to the effective stress* in the ligament can be calculated as a function of x/T by using the principal stress values given in Equation (1).

The estimate of the plastic instability stress in the ligament is rather arbitrary. However, low carbon steels, such as ASTM A106B, commonly exhibit a rather sharp tensile yield point, and it is assumed that the effective instability stress for such a material is approximately equal to its uniaxial tensile yield stress.

The validity of the plastic instability hypothesis has been tested with experimentally determined burst hoop stress values for ASTM A106B pipes containing long part-through flaws.[1] Ratios of burst hoop stress to uniaxial tensile yield stress have been compared with hoop stress to effective stress ratios calculated by using the principal stress values given in Equation (1). Considering the rather arbitrary choice of a value for σ_3 and the effective instability stress, reasonable agreement was obtained over a considerable range of x/T.

*Effective stress $\bar{\sigma}$ is defined by $\bar{\sigma} = \frac{1}{\sqrt{2}}\sqrt{(\sigma_1 - \sigma_2)^2 + (\sigma_1 - \sigma_3)^2 + (\sigma_2 - \sigma_3)^2}$.

2.2 BEHAVIOR OF PIPES WITH AXIAL THROUGH-WALL FLAWS

The failure stress for a wide plate of brittle material containing a through-wall crack and under uniaxial tension normal to the crack plane is given by the relation

$$\pi\sigma^2 c = K_{Ic}^2 \tag{2}$$

where:

σ = applied stress,
c = crack half-length, and
K_{Ic} = material constant.

The so-called plane strain fracture toughness or critical stress intensity factor is defined by linear elastic fracture mechanics.[2] If the material is not completely brittle, Equation (2) must be corrected by a term which is a function of the ratio of K_{Ic} to the yield stress of the material. Dimensionally, the equation is unchanged; i.e., the limiting stress that the plate will sustain varies inversely as the square root of the crack length. The fracture mechanics analysis indicates that a tensile stress component parallel to the crack should not affect the value of the instability stress normal to the crack plane; thus, a crack in a very large diameter thin-wall cylindrical shell under internal hydrostatic pressure should approach the behavior of the crack in a wide thin plate under uniaxial tension equal to the hoop stress. However, as the diameter of the shell decreases and crack length increases, it is necessary to take into account bending stresses about the crack. Anderson[3] used dimensional reasoning and developed an expression of the form

$$\sigma^2\left[\pi c + \frac{1}{2}\left(\frac{K_c}{\sigma_B}\right)^2\left(1 + q\,\frac{c}{R}\right)\right] = K_c^2 \tag{3}$$

where:

K_c = nominal stress intensity factor,
σ_B = biaxial yield stress,
c = crack half-length,
R = cylinder radius,
σ = membrane hoop stress at instability, and
q = "bulge coefficient" dependent on material properties and cylinder radius.

Irvine, Quirk, and Bevitt[4] used experimental data from tests on 5-foot-diameter pressure vessels and concluded that the load limit for a thin-wall cylinder under internal pressure was given by an expression of the form

$$\sigma^3 c^2 = K \tag{4}$$

where K is a constant dependent on ultimate strength, yield strength, and the Charpy impact energy of the material. The form of the relationship between this constant and the material properties of the material was dependent on the fracture mode observed.

Eiber and co-workers[5] developed an expression based chiefly on an earlier work of Folias,[6] which takes into account both bending stresses and plastic zone correction and gives an effective critical stress intensity factor or crack toughness for axially cracked pipes in terms of hoop stress and crack length. This expression is of the form

$$K^2 = \frac{\pi c \sigma_h^2}{\cos\theta}\left(1 + \frac{5\pi}{32}\lambda^2\right)\left(\frac{4-k}{2}\right) \tag{5}$$

where:

K = stress intensity factor, ksi $\sqrt{\text{in.}}$,
c = crack half-length, inches,
$\lambda^2 = \frac{c^2}{Rt}\sqrt{12\,(1-\nu^2)}$,

ν = Poisson ratio,
R = radius of vessel, inches,
t = wall thickness, inches,
$\theta = \frac{\pi}{2}\frac{\sigma_h}{\sigma_o}$,
σ_h = nominal hoop stress, ksi,
σ_o = failure hoop stress for unflawed vessel, ksi, and
k = $(3-4\nu)$ plane strain; $(3-\nu)/(1+\nu)$ plane stress.

This equation, intended to be chiefly applicable to large diameter pipes, has been applied by Eiber to the fracture behavior of axially flawed low carbon steel pipes for which the product of radius and wall thickness is 20 inch^2 or more. It will be observed that for flaws short in comparison to Rt. Equation (5) reduces to the typical elastic fracture mechanics form

$$\sigma^2 c = \text{constant}; \tag{6}$$

while for long flaws, the form

$$\sigma^2 c^3 = \text{constant} \tag{7}$$

is approached. The Irvine, Quirk, and Bevitt relation lies between these extremes. As flaw size decreases, the factor $1/\cos\theta$ in Equation (5) increases rapidly and becomes quite sensitive to small errors in either σ_h or σ_o.* Recently, Eiber has reported[7] that Equation (5) does not fit experimental test data as well as the simpler relation

$$\sigma_f^2 = \sigma_h^2\left(1 + 1.62\,\frac{c^2}{Rt}\right) \tag{8}$$

where σ_f is defined as a flow stress and other quantities are as in Equation (5). The value of σ_f has been found to be between tensile yield and ultimate stresses for the pipe material.

2.3 PIPES WITH SHORT PART-THROUGH FLAWS

The pressure load maximum for a pipe containing a short part-through flaw is not so simply related to plastic instability in the ligament at the base of the flaw as it appears to be for long flaws. The series-connected tensile element analogy obviously does not apply to the short flaw case, and more sophisticated computer techniques for dealing with the problem remain to be developed. Experimental tests on specimens containing artificially prepared flaws appear to be the most economical source of information on the behavior of short axial part-through flaws in pipes. Because of the two-dimensional nature of such flaws as contrasted to the axial through-wall or long part-through flaw, considerably more data are needed to treat empirically the short, through-wall flaw than are needed (for example) to adjust the constants in a relation such as Equation (3).

2.4 CIRCUMFERENTIALLY FLAWED PIPES UNDER BENDING STRESSES

The axial membrane stress in a thin-walled cylindrical vessel due to internal fluid pressure is equal to one-half the circumferential stress. As a consequence, the pressure burst strength of a pipe or cylindrical vessel is rather insensitive to circumferential flaws. Pressure burst tests on circumferentially flawed ASTM A106B pipes show that unless the circumferential flaw is rather severe, failure is caused by axial splitting rather than by circumferential extension of the flaw. Figure 1 shows an example of this behavior—a pipe which contained a 36 degree through-wall axial flaw, yet failed by axial cracking. Tests on pipes with 360 degree part-through circumferential flaws of constant depth show that the burst pressure of a pipe is not reduced unless the flaw depth exceeds one-half the pipe wall thickness. The circumferential-to-axial-stress ratio in a pressurized pipe thus weighs rather strongly against the failure of a pipe with a circumferential flaw, unless the flaw is very severe or bending stresses are also present. Approximate stress intensity factors can be calculated for circumferentially flawed pipes under bending loads. Harris[8] has developed an expression for the elastic stress intensity factor applicable to a pipe containing a complete (360 degree) circumferential part-through flaw of constant depth:

*The term $1/\cos\theta$ goes to infinity as c approaches zero; however, the term $c/\cos\theta$ should approach the value $K^2/\pi\sigma_o^2$.

$$K_I = \frac{F}{\pi\left[(c + a)^2 - c^2\right]} \sqrt{\frac{\pi t}{0.80 + \frac{t}{a + c}\left(4 + 1.08\,\frac{c}{a}\right)}} + \frac{4M\,(c + a)\cos\phi}{\pi\left[(c + a)^4 - c^4\right]} \sqrt{\frac{\pi t}{0.80 + \frac{t}{a + c}\left(7.12 + 1.08\,\frac{c}{a}\right)}} \tag{9}$$

where:

F = applied tensile load,
M = applied bending moment,
a = ligament depth,
t = flaw depth,
c = pipe inside radius,
ϕ = angular coordinate,
a + t = pipe wall thickness, and
K_I = opening-mode stress intensity factor.

Gilman[9] has developed an expression for the stress intensity factor K_c in a pipe containing a short circumferential through-wall flaw and under a combined pressure and bending stress:

$$K_c = \sqrt{\pi c}\left[\frac{PR_o}{2t} f_1\ (c) + \frac{M}{\pi R^2 t} f_2\ (c)\right] \tag{10}$$

where:

c = crack half-length,
P = pressure at failure,
M = bending moment at failure,
t = pipe wall thickness,
R = pipe mean radius,
R_o = pipe inside radius, and
f_1, f_2 = correction factors for bulging.

There is some uncertainty as to the values of f_1 and f_2 to be used in the calculation, but appropriate values for the crack lengths in question can be estimated from the Folias[10] relation with an error of probably less than 10%.

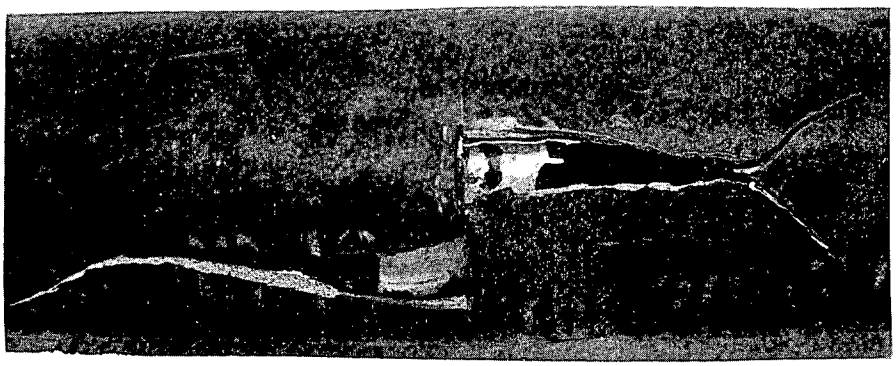

Figure 1. Axial Fracture in Circumferentically Flawed Pipe

3. EXPERIMENTAL PROCEDURES

The work to be reported has been limited to specimens of ASTM A106B pipe in sizes ranging from 4 to 12 inches nominal diameter and to ASTM A234B tees and elbows of 6-inch Schedule 80 size. Pipe specimens consisted of segments of length greater than four diameters closed at the ends with standard welding caps of the same material. Fitting specimens were welded to 1-foot segments of A106B pipe, which were, in turn, welded to standard welding caps. Pipe specimens containing both through-wall and internal and external part-through flaws were tested. Fitting specimens were limited to external part-through flaws in the configurations shown in Figure 2.

Part-through flaws in pipes were cut chiefly with a 2.75-inch-diameter, 45 degree Vee milling cutter with a 0.010-inch tooth tip radius. Earlier in the program, short part-through flaws were cut in some specimens with slitting saws or abrasive wheels ranging from 0.015 to 0.020 inch in thickness. Full-length axial flaws have been cut with milling cutters ranging from 0.020 to 0.188 inch in thickness.*

Axial through-wall flaws of varying lengths were cut in the centers of the specimens with a saber saw. The ends of the flaws were sharpened either by hand-broaching to a tip radius of approximately 0.001 inch or by cyclic pressurization of the specimen until visible fatigue crack propagation had occurred. Before welding the end caps on these specimens, each flaw was sealed with a laminated patch consisting of a layer of 1/32-inch-thick annealed aluminum next to the pipe wall and extending approximately 2-1/4 inches beyond the flaw in each direction, a somewhat smaller piece of 1/16-inch-thick annealed mild steel, and finally a piece of 1/16-inch-thick Neoprene extending about 1 inch beyond the edges of the aluminum. The patch was formed to the proper curvature and assembled outside the pipe with General Electric RTV 102 cement between metal layers and RTV 90 cement between the Neoprene and the metal. After curing, the completed patch was cemented in place with RTV 90 cement between the Neoprene sheet and the pipe wall. While the cement was curing, the patch was held in place in the pipe by an inflated rubber bladder, and the pipe was warmed slightly with an infrared lamp.

The specimens were tested hydrostatically with water or water-ethylene glycol mixtures as the pressurizing fluid. Hydrostatic pressure was generated with an air-driven, piston-type booster pump with a piston area ratio of 300 to 1. An electrical contact built into the end of the driving cylinder closed when the piston was fully retracted. Pressure applied to the specimen was measured by a strain-gage-type pressure transducer connected through an appropriate signal conditioner to a strip-chart potentiometer recorder. The chart paper on the recorder was advanced by a solenoid-driven ratchet motor actuated by electrical pulses from the contact on the pump. It was found that the volume of water delivered per stroke of the pump was essentially constant over the pressure range covered in the tests. Since chart motion was proportional to the number of pump strokes, the recorder produced a plot of applied pressure against volume of water delivered to the specimen. If the compressibility of water is neglected, the chart record amounted to a plot of load versus deformation for the specimen. In early experiments of the test series, specimen deformation was measured by post-yield strain gages attached in a cir-

* Burst hoop stress was found to be strongly dependent on flaw depth and rather insensitive to flaw width.

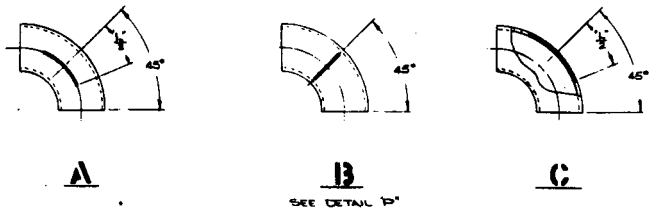

TYPES OF ELBOW FLAWS

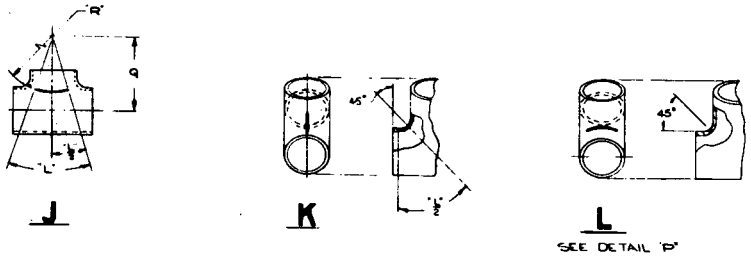

TYPES OF TEE FLAWS

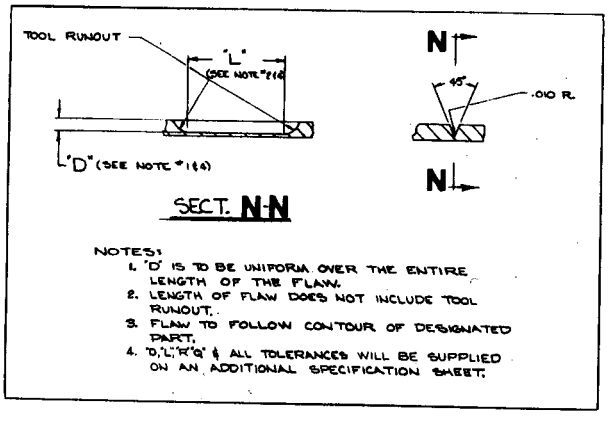

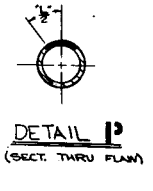

Figure 2. Flaw Configurations in Fitting Specimens

cumferential direction to the mid-portion of the pipe specimen approximately 90 degrees from the flaw. After development of the volume recorder, strain gages were not used, and general plastic deformation of the specimen was determined by pre- and post-test measurements of pipe circumference. Unflawed pipes were tested to obtain load maxima in the absence of defects.

Material

ASTM A106B seamless pipe is made of steel of 0.30% nominal carbon content, and is neither isotropic nor particularly uniform with respect to mechanical properties. The material used in these tests was intended to be representative of routine manufacturing practice; no effort was made to select it on a basis of special properties. Mechanical tests of the material were limited to tensile tests and Charpy impact fracture tests with either full-size specimens or subsize specimens when specimen size was limited by pipe wall section thickness. Figure 3 contains data from a single length of 6-inch Schedule 80 pipe which are illustrative of the toughness anisotropy of this material. The room temperature tensile properties of the material used and the burst hoop stress for unflawed pipe of each size are given in Table 1.

Table 1
ROOM TEMPERATURE TENSILE PROPERTIES OF ASTM A106B PIPE USED IN PRESSURE LOAD LIMIT TESTS

Size (inch) and Schedule	Specimen Direction	0.2% Yield Stress (ksi)	Ultimate Stress (ksi)	Percent Elongation	Burst Hoop Stress,* (ksi)
12-80	C	45.8	68.6	31.0	61.2
10-40	L	38.9	64.3	35.0	–
10-40	C	38.2	65.0	30.4	56.3
10-80	L	38.4	72.2	32.2	–
10-80	C	48.9	73.5	26.5	66.0
8-40	L	48.8	74.6	28.4	–
8-40	C	50.3	76.2	27.9	69.4
8-80	L	41.3	67.3	29.6	–
8-80	C	44.6	68.1	26.0	62.2
6-40	L	41.2	61.1	37.0	–
6-40	C	43.8	62.6	30.4	62.0
6-80(a)	L	39.7	65.5	34.0	–
6-80(a)	C	45.3	66.5	27.4	58.8
6-80(b)	C	50.0	67.3	25.5	65.4
4-160	L	37.4	70.0	33.7	–
4-80	L	44.2	72.8	32.2	–
4-40	L	43.3	68.8	32.7	57.7
3-160	L	38.0	62.9	32.7	–
3-80	L	45.0	64.2	33.4	–
2-160	L	49.4	80.2	27.5	–
2-80	L	52.2	73.5	25.6	–

C = Circumferential
L = Longitudinal

(a) and (b) indicate two distinct heats in this size

*For an unflawed pipe specimen based on original dimensions.

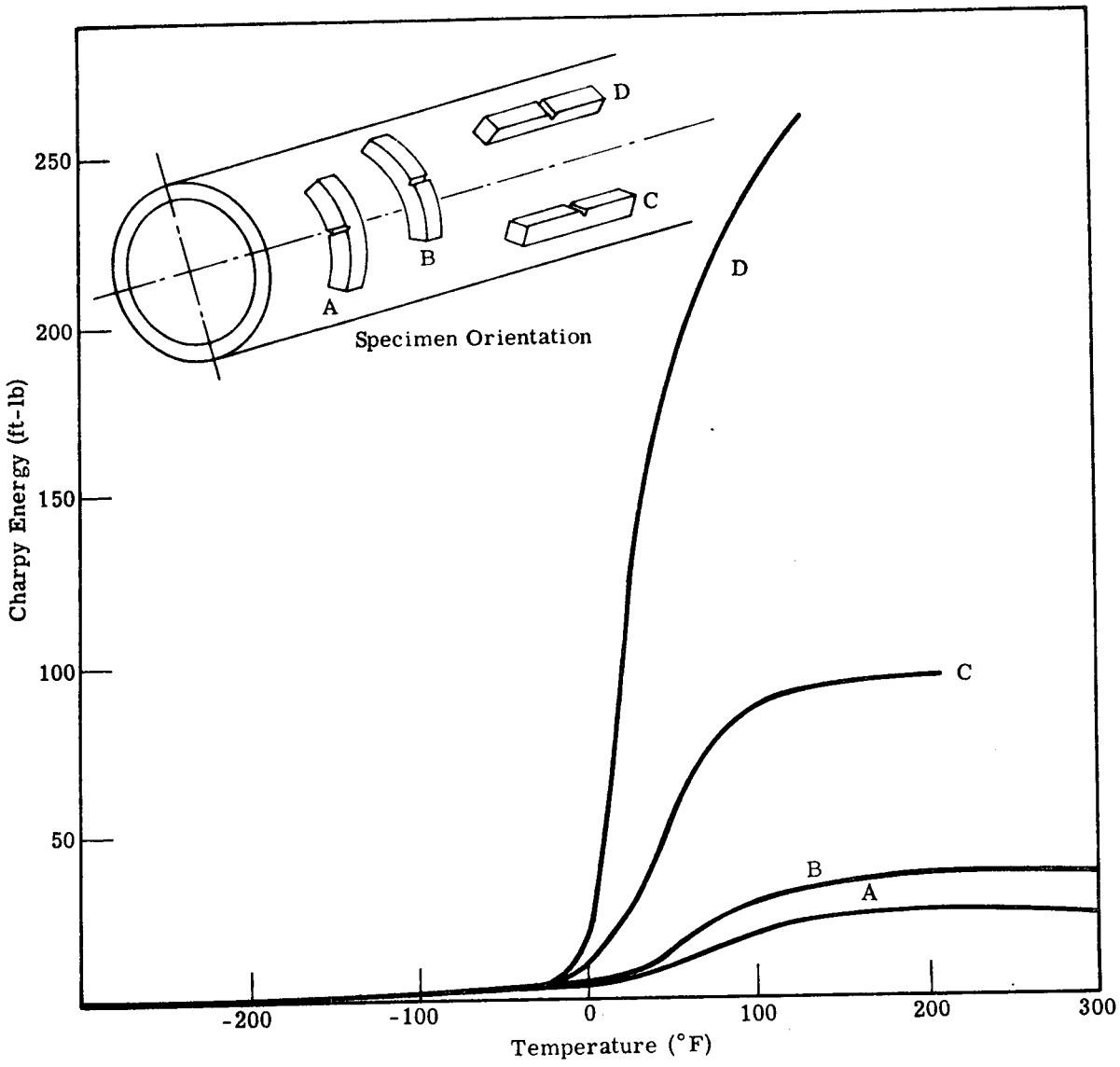

Figure 3. Toughness Anisotropy of ASTM A106B Pipe

4. EXPERIMENTAL RESULTS

4.1 PIPES WITH AXIAL THROUGH-WALL FLAWS

Twenty-five specimens of A106B pipe in various diameters and wall thickness with axial through-wall flaws of different lengths were tested. Typical failure appearances are shown in Figure 4. A plot of maximum hoop stress versus flaw half-length for six different pipe sizes is presented in Figure 5. If the load maximum was not reached first, general yielding occurred at hoop stresses equal to approximately 1.15 times the uniaxial tensile yield stress, as would be predicted from theory. There was no evidence that the behavior of fatigue-sharpened flaws differed from that of the hand-finished flaws. Data points for each size of pipe are consistently above or below the drawn curve. The relative position of these points with respect to the curve cannot be accounted for by the corresponding heat-to-heat variation in mechanical properties as given in Table 1. If maximum hoop stress is plotted against flaw half-length divided by pipe mean radius, the spread of data points about the drawn curve is reduced somewhat (Figure 6). The dotted line in Figure 6 indicates the code allowable stress for ASTM A106B pipe at room temperature. The intersection of this line with the curve indicates that a flaw of length approximately equal to the pipe diameter is needed to reduce the load maximum under monotonic loading to the level of the code allowable stress.

Values of effective critical stress intensity factor or fracture toughness were calculated from the load maximum data by using Equation (5). These values are plotted against flaw half-length in the upper part of Figure 7. The increase in K with increasing flaw length is not surprising since the authors of the equation make no claim for its validity at large values of c^2/Rt. By experimentation it was found that an empirical equation of the form

$$K^2 = \frac{\pi \sigma_h^2 c}{\cos \theta} \left(1 + 0.4 \frac{c^2}{Rt}\right) \tag{11}$$

greatly reduced the variation in K with flaw length. Values of K calculated by using Equation (11) are shown in the lower part of Figure 7. Again, there is no obvious correlation between the scatter in the values of K about the mean value of 95.6 ksi $\sqrt{\text{in.}}$ and the heat-to-heat variation in either tensile yield stress or the burst hoop stress for pipe in the unflawed condition.

Flow stress (σ_f) was calculated from the test data with Equation (8). A plot of these values, divided by the average of the yield and ultimate tensile stresses, versus flaw half-length is shown in Figure 8. Comparison with Figure 7 shows that the scatter of data points about the drawn curve is about the same in each case.

4.2 PIPES WITH AXIAL PART-THROUGH FLAWS

Results of tests on pipes containing short part-through external axial flaws are shown in Figure 9. In this figure, pressure load limit or burst pressure, expressed as a fraction of that for an unflawed pipe is plotted against the reciprocal of corrected flaw length.* The upper dotted line represents the unflawed condition, for which x/T equals unity.** The lower curve represents the behavior of pipes with through-wall axial flaws for which x/T is equal to zero. Load maxima for pipes with full-length flaws ($1/L \simeq 0$) are plotted along the ordinate at the left of the diagram at heights dependent on the value of x/T; all points representing load maxima for pipes having short part-through flaws lie between the curve and the upper line at locations dependent on the x/T value for the particular flaw. Flaws with low values of x/T lie near the curve; high values (shallow flaws) give points near the upper line. In Figure 9, dotted lines have been drawn to give estimates of load limit values for x/T equal to 1/4, 1/2, and 3/4, respectively. As was the case for through-wall flaws discussed above, there is considerable scatter in the data points although the trends indicated by the dotted lines are evident. To eliminate the effect of pipe-to-pipe property variations, two 20-foot lengths of pipe were cut into test specimens. Specimens with both inside and outside flaws were cut from each pipe as was one unflawed control specimen. Test data from these two pipes, designated as numbers 18 and 19, are given in Figure 10, as are the data from inside-flawed specimens from another pipe. The improvement in

* This correction was necessary because flaws were machined with a round cutter and were not of full depth at the ends. Corrected length is length of a flaw having full depth at the ends and subtending area equal to machined flaw.

**Here T represents the pipe wall thickness and x the thickness of the ligament at the base of the flaw.

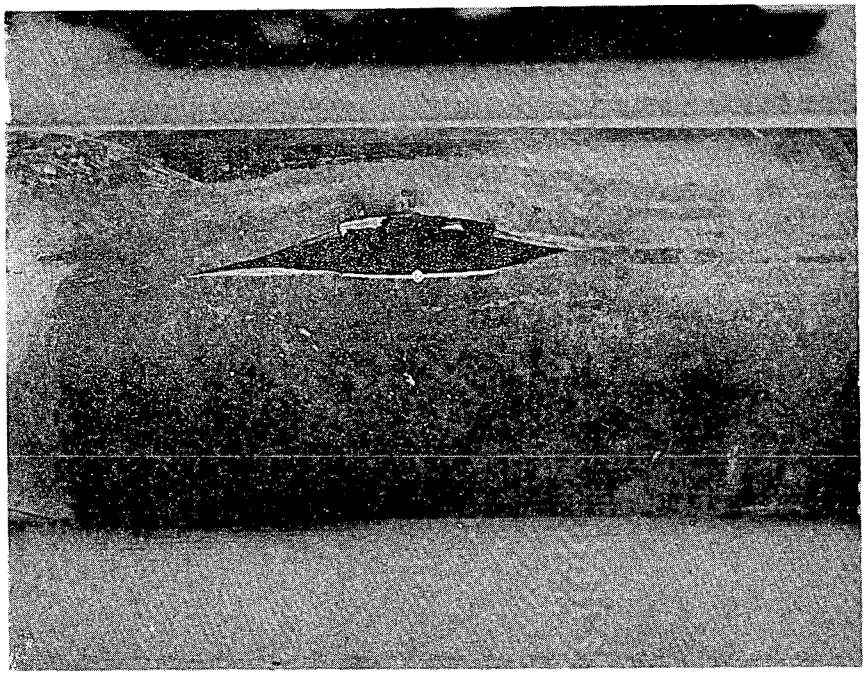

a. 8-inch Schedule 40, 3-inch Flaw
Maximum Hoop Stress 31.8 ksi

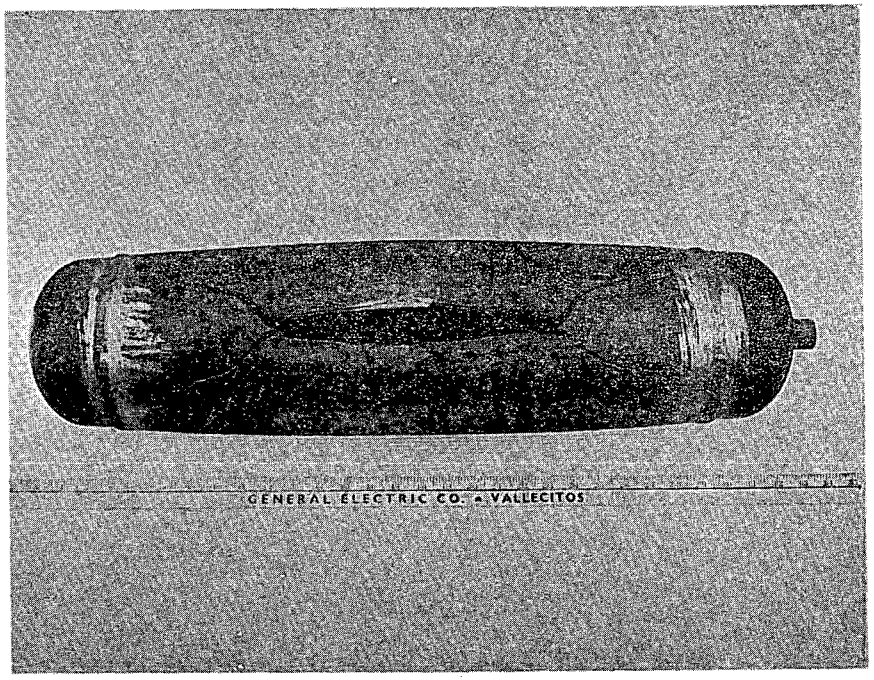

c. 6-inch Schedule 80, Unflawed
Maximum Hoop Stress 58.8 ksi

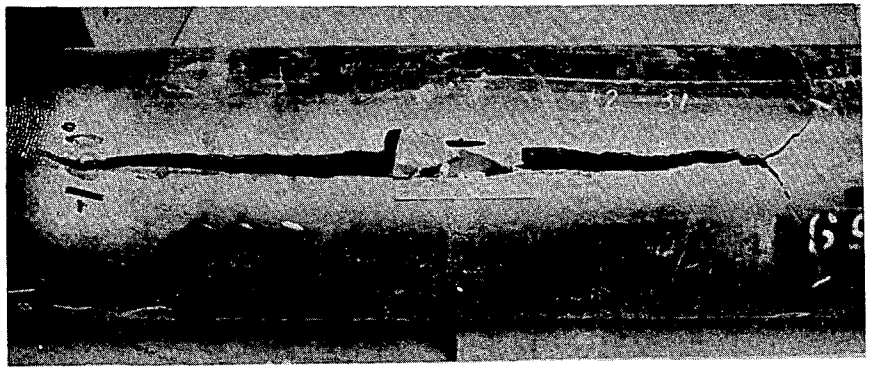

b. 12-inch Schedule 80, 2-inch Flaw
Maximum Hoop Stress 38.4 ksi

d. 6-inch Schedule 80, 8-inch Flaw
Maximum Hoop Stress 10.3 ksi

Figure 4. Typical Failure Behavior in Hydrostatic Tests of ASTM A106B Pipe

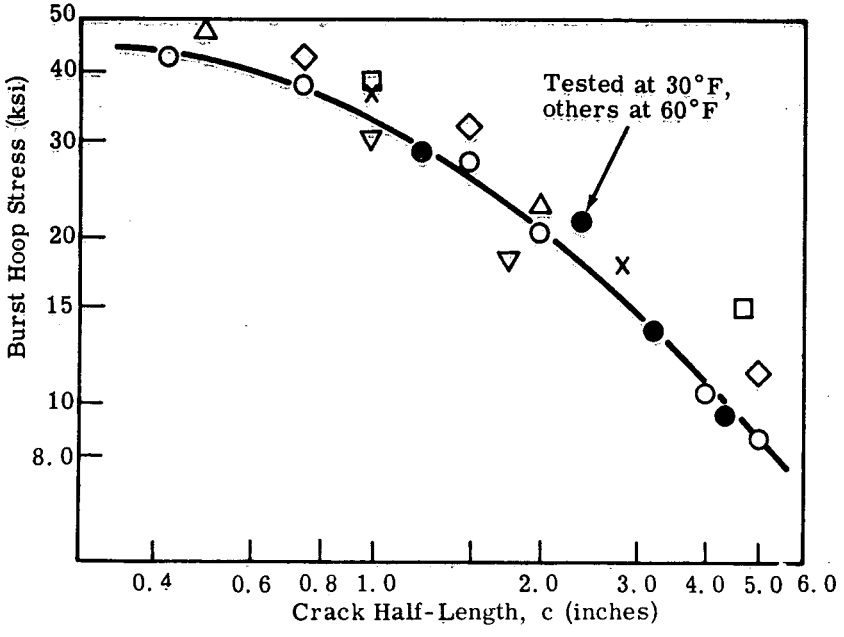

	Diameter	Schedule	R	t	R/t	Rt
▽	4	40	2.10	0.23	9.15	0.48
△	6	40	3.20	0.28	11.4	0.90
●○	6	80	3.12	0.43	7.26	1.34
◇	8	40	4.17	0.32	12.8	1.35
X	10	40	5.22	0.36	14.5	1.88
□	12	80	6.04	0.71	8.51	4.28

Figure 5. Variation of Pressure Load Limit with Flaw Length in ASTM A106B Pipe with Axial Through-Wall Flaws

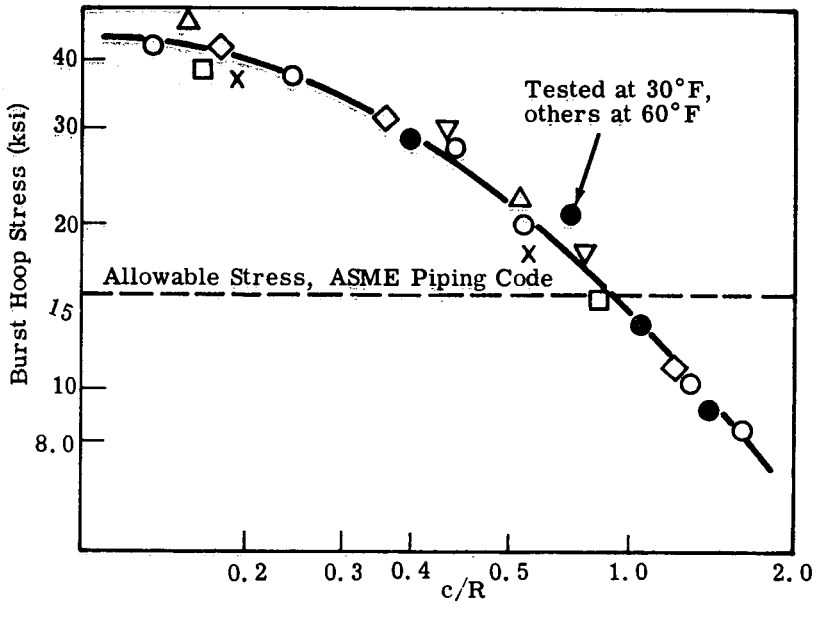

	Diameter	Schedule	R	t	R/t	Rt
▽	4	40	2.10	0.23	9.15	0.48
△	6	40	3.20	0.28	11.4	0.90
●○	6	80	3.12	0.43	7.26	1.34
◇	8	40	4.17	0.32	12.8	1.35
X	10	40	5.22	0.36	14.5	1.88
□	12	80	6.04	0.71	8.51	4.28

Figure 6. Pressure Load Limit Versus c/R for ASTM A106B Pipe with Axial Through-Wall Flaws

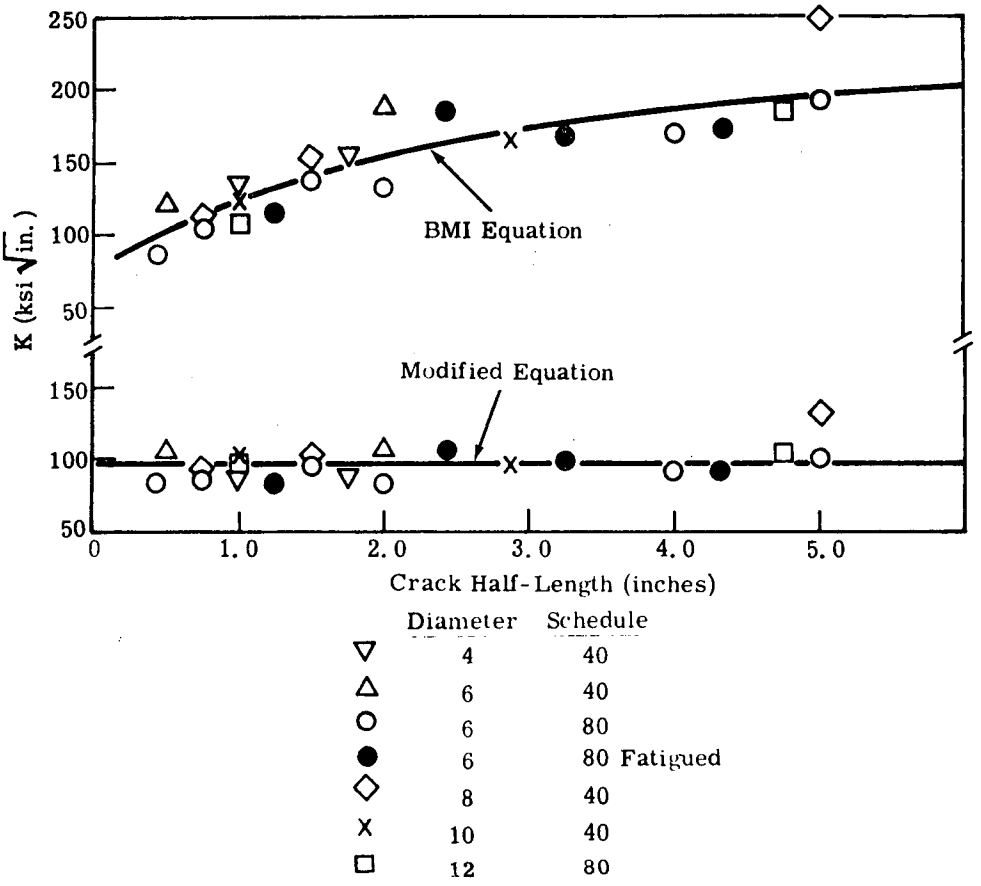

Figure 7. Effective Critical Stress Intensity Factor for ASTM A106B Pipes Containing Axial Through-Wall Flaws

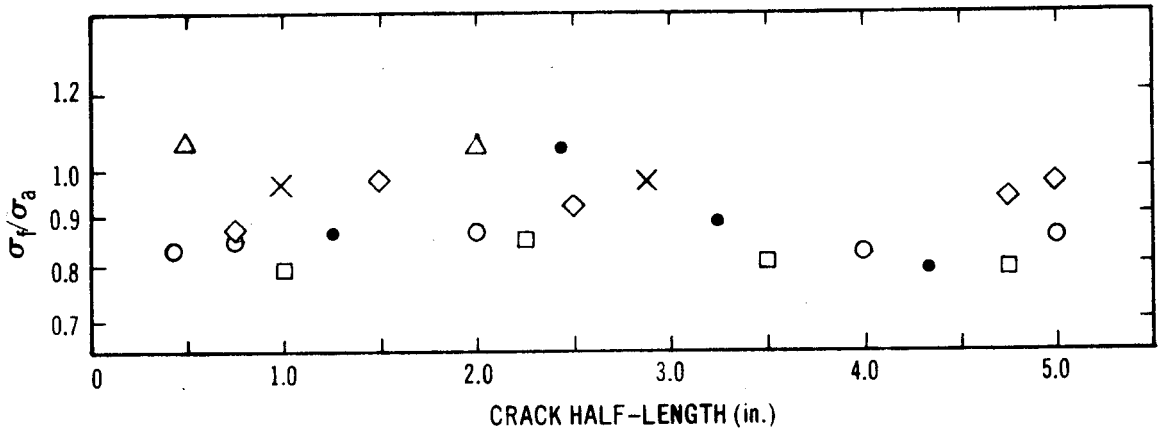

	DIAMETER	SCHEDULE	R	t	R/t	Rt
▽	4	40	2.10	0.23	9.15	0.48
△	6	40	3.20	0.28	11.4	0.90
● ○	6	80	3.12	0.43	7.26	1.34
◇	8	40	4.17	0.32	12.8	1.35
×	10	40	5.22	0.36	14.5	1.88
□	12	80	6.04	0.71	8.51	4.28

Figure 8. σ_f/σ_a Versus Crack Half-Length, ASTM A106B Pipe

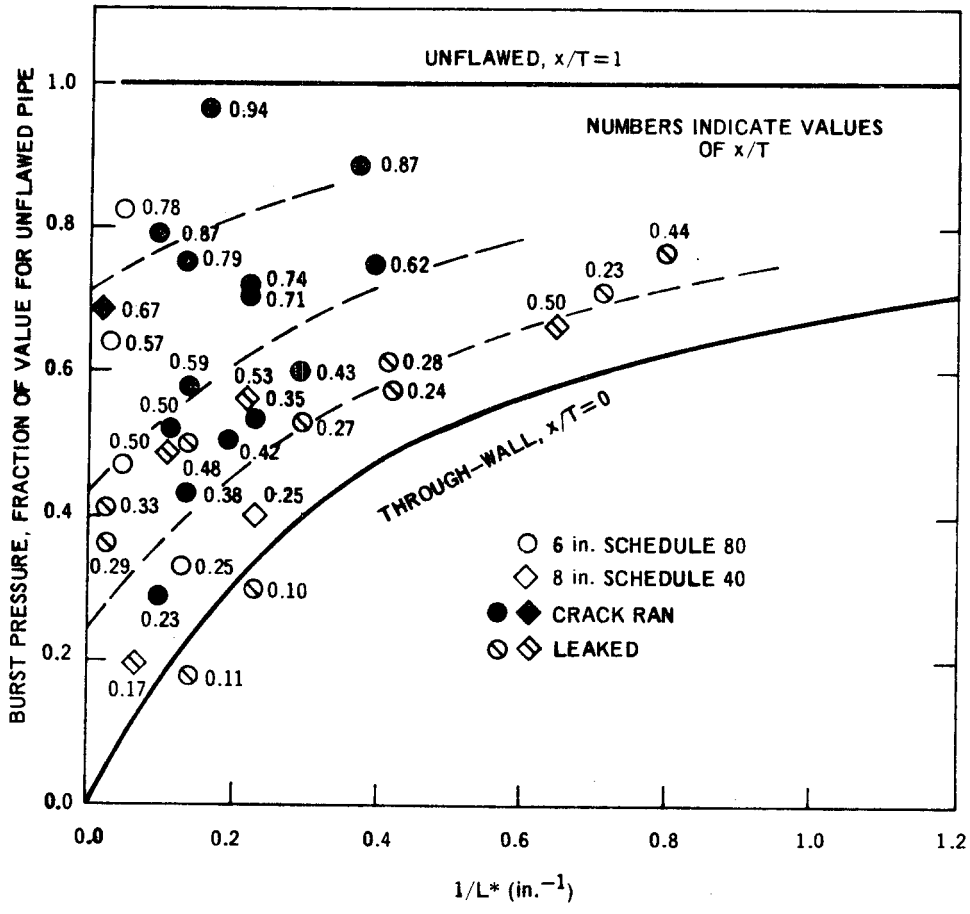

Figure 9. Failure Diagram for ASTM A106B Pipe, Part-Through Flaws

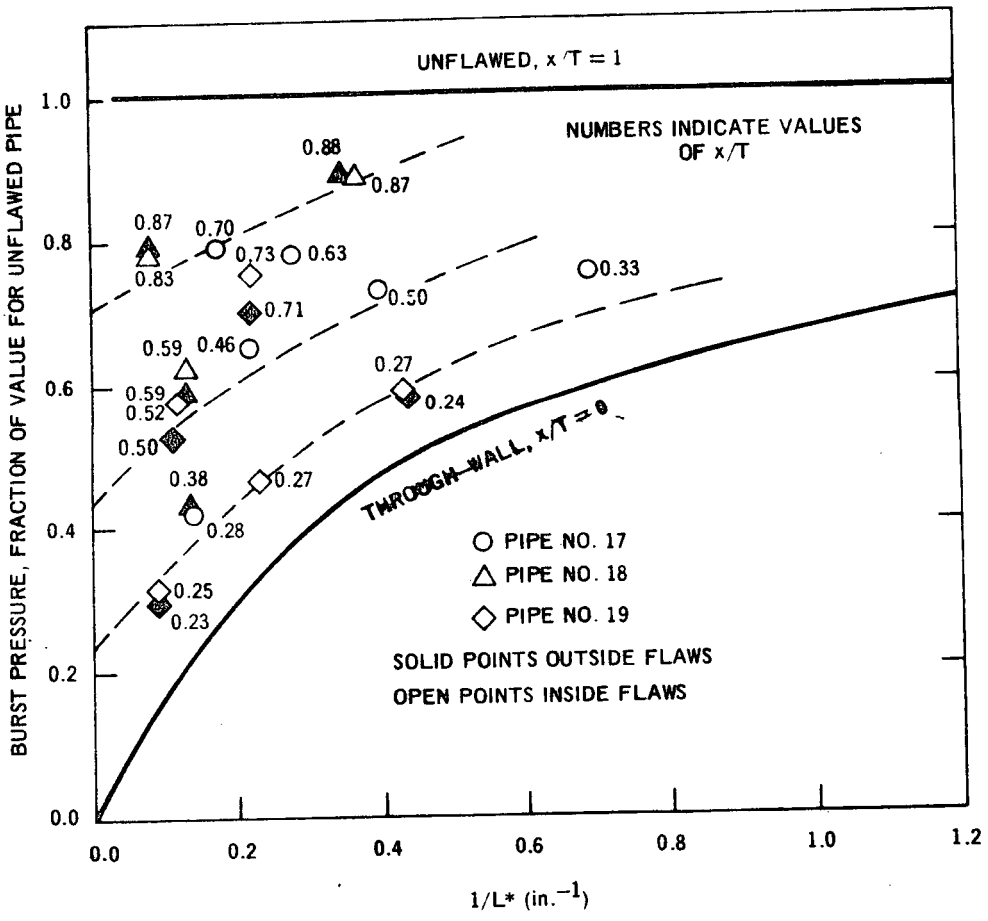

Figure 10. Comparison of Inside with Outside Flaws

consistency compared to the data illustrated in Figure 9 is apparent. Also, it is apparent that the reduction in strength resulting from an inside flaw is equivalent to that from an external flaw of the same size and depth.

4.3 PIPES WITH CIRCUMFERENTIAL FLAWS

Because the axial stress in a pressurized, thin-walled, cylindrical vessel is but one-half the circumferential stress, it may be expected that the reduction in pressure load limit due to a circumferential flaw will be less than that due to an axial flaw of comparable size. This is indeed the case, as seen in Table 2, which lists the pressure load limits for a number of specimens of ASTM A106B pipes containing circumferential flaws of various configurations. In each case, the specimen was tested using water, or a mixture of water and ethylene glycol, as the pressurizing medium. With the exception of the tests involving bending moments, all tests were conducted at approximately 60°F. In all specimens, except those containing the most severe flaws, the hoop stress reached levels sufficient to cause general yielding before the stress intensity in the direction normal to the flaw reached the instability level.

To study the failure of circumferentially flawed pipes under bending stresses, four pipes were tested under bending loads. The experimental configuration used for testing specimens under combined bending and pressure loading is shown schematically in Figure 11. In each case, the bending load was applied at a point approximately 33 inches from the flaw location. The hydraulic cylinder, of a 3.25-inch piston diameter, was actuated by an electrical pump in conjunction with a spring-loaded pressure relief valve to maintain the bending load at any desired constant value.

Test data for pipes tested under bending loads with or without simultaneous pressure loads are given in Table 3.

The condition of the specimens (6-63-8B and 6-64-8B) after test is shown in Figures 12 and 13. Both specimens failed by sudden propagating fracture once the load limit was reached. After a bending moment of approximately 6.6×10^5 pound-inches was applied to specimen 6-63-8B, the load was removed to inspect the ends of the 4-inch through-wall flaw. A plastic displacement (COD) of approximately 0.10 inch had occurred at the ends of the flaw. Upon reloading, failure occurred suddenly around the full circumference at an applied moment of 6.50×10^5 pound-inches. The fracture surface was found to be perpendicular to the maximum principal stress, with minimal shear lips. In each case, the applied load at the moment of brittle fracture was grossly in excess of what would be permitted by design codes.

For comparison with data from axially flawed pipes, approximate elastic critical stress intensity factors were calculated for the pipes tested under bending loads, using either the Harris[8] or the Gilman[9] relation, depending on flaw type. If the toughness anistropy of the pipe shown by the Charpy tests is considered, the K_c values of 133 and 147 ksi$\sqrt{\text{in.}}$ for the circumferential through-wall flaws is not inconsistent with the value of 96 ksi$\sqrt{\text{in.}}$ obtained for axial through-wall flaws. The behavior of the pipes with complete part-through flaws is clearly not consistent with the Harris formula, as would be expected, considering that necking preceded failure on the side of the pipe wall opposite the flaw.

4.4 FAILURE BEHAVIOR OF FLAWED TEES AND ELBOWS

Test procedures for flawed tees and elbows were identical to those used for straight segments of pipe. Test data and results for the specimens tested are given in Table 4. Pressure load limits are expressed as a fraction of the burst pressure of an unflawed fitting in conjunction with the short segments of pipe welded to it. Wall thicknesses of tees and elbows are greater than in matching pipe of the same schedule in order to compensate for geometrical stress concentration. In hydrostatic tests of an unflawed tee and an unflawed elbow at 60°F, failure in each case initiated as a shear fracture in a crotch of the fitting and propagated into the attached pipe as an axial brittle fracture, as shown in Figures 14, 15, and 16.

Figures 17 and 18 show resultant failures from testing flawed elbows and tees, respectively. Under each photograph is given the failure pressure, P/P_o as a fraction of that for an unflawed fitting, the flaw length, L, measured at the pipe surface, the average wall thickness, T, at the flaw location, and the fraction, x/T, of wall thickness remaining at the base of the flaw.

If failure pressure data for flaws of types A and C in elbows (see Figure 2) are compared with pipe data by interpolation in Figure 9, it is seen that somewhat deeper flaws are required to produce a given reduction in failure pressure in elbows than are required in straight pipe segments. There are two reasons for this: the slightly greater wall thickness in the elbow and the difference in principal stress ratios. By use of strain gages on unflawed specimens it was found that the circumferential to axial elastic stress ratio was approximately 1.5 in the location of a type A flaw and 1.7 in the location of a type C flaw, compared to 2.0 in the wall of a straight pipe.

Analysis of the flawed tees on a basis of either linear elastic fracture mechanics or the unstable plastic ligament concept was not attempted because of difficulties in defining the stress fields about the flaws. It was found that tees were quite sensitive to flaws of types J and K and (in the absence of bending stresses) almost completely insensitive to flaws of type L.

Table 2
PRESSURE LOAD LIMITS FOR CIRCUMFERENTIALLY FLAWED PIPES

Specimen Number	Size and Schedule	Outside Diameter	Wall Thickness, T (in.)	Burst Pressure (ksi)	Pressure Load Limit**	Flaw Configuration	Flaw Length (degrees)	x/T*	Remarks
6-20-8	6 in. - 80	6.66	0.434	9.79	1.00	0.020-in. Milled slot, outside	360	0.72	General yielding prior to axial failure
6-21-8	6 in. - 80	6.66	0.429	8.60	0.98	0.020-in. Milled slot, outside	360	0.55	General yielding prior to circumferential failure
6-22-8	6 in. - 80	6.67	0.429	4.81	0.55	0.020-in. Milled slot, outside	360	0.18	Circumferential failure
6-23-8	6 in. - 80	6.66	0.435	9.20	1.00	Through-wall, 0.050 in. wide	34	0.00	Split axially after general yielding
6-24-8	6 in. - 80	6.66	0.432	7.74	0.88	0.020-in. Milled slot, outside	360	0.38	General yielding prior to circumferential failure
6-25-8	6 in. - 80	6.66	0.436	8.20	0.93	Through-wall, 0.050 in. wide	68	0.00	Split axially after general yielding
6-26-8	6 in. - 80	6.66	0.428	9.42	–	0.020-in. Milled slot, outside	360	0.52	Type-304 stainless steel, 22% circumferential strain at failure
8-20-4	8 in. - 40	8.66	0.321	4.275	0.76	0.020-in. Milled slot, outside	360	0.39	General yielding, circumferential failure
6-29-I-8	6 in. - 80	6.68	0.449	8.58	–	45° Vee, inside	180	0.33	Split axially and circumferentially

*T = Wall thickness
x = Ligament thickness
**Expressed as fraction of value for an unflawed pipe.

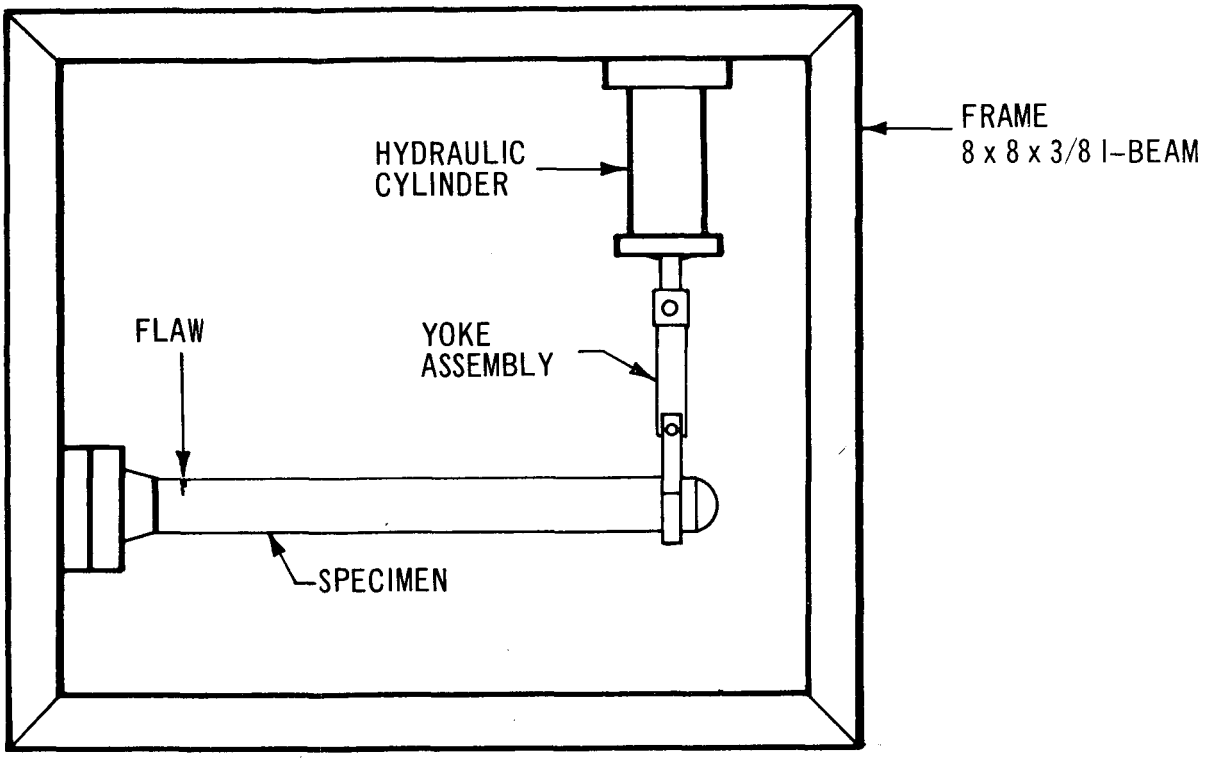

Figure 11. Test Assembly, Schematic

Table 3
BEHAVIOR OF CIRCUMFERENTIALLY FLAWED PIPES UNDER BENDING AND PRESSURE STRESSES

Specimen Number	6-22-8	6-27-8B	6-28-8B	6-63-8B	6-64-8B
Test Temperature, °F	60	74	89	75	70
Flaw Length	360°	42.7°	360°	68.6°	360°
x/T(a)	0.18	0.0	0.70	0.0	0.475
Burst Pressure, ksi	4.81	6.00	6.52	0	0
Burst Moment, 10^5 lb-in.	0	5.49	6.60	6.50	6.62
K_p, ksi$\sqrt{\text{in.}}$ (b)	37.9	40.6	17.7	0	0
K_B, ksi$\sqrt{\text{in.}}$ (b)	0	92.2	40.7	147	64.6
K_c, ksi$\sqrt{\text{in.}}$ (b)	37.9(c)	133	58.4	147	64.6(c)
Flaw Type	0.020-in. slit	0.045-in. slit	0.020-in. slit	0.045-in. slit	45° vee

(a) x = Ligament thickness
T = Wall thickness

(b) $K_p + K_B = K_c$.
These subscripts refer to pressure, bending, and critical, respectively.

(c) Low values because of inappropriate formulation for K (see text) for 360-degree flaws.

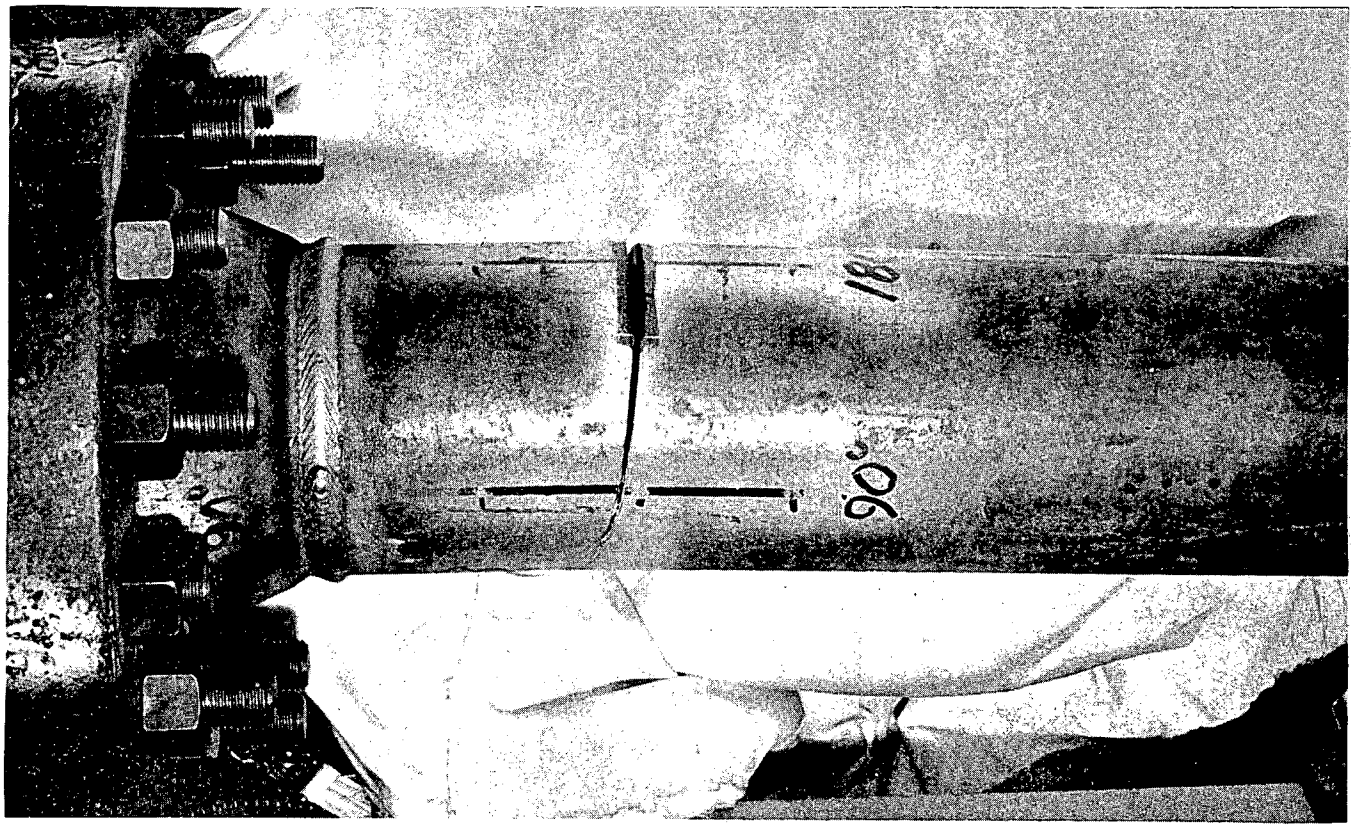

Figure 12. Pipe with Through-Wall Flaw, Bending Only

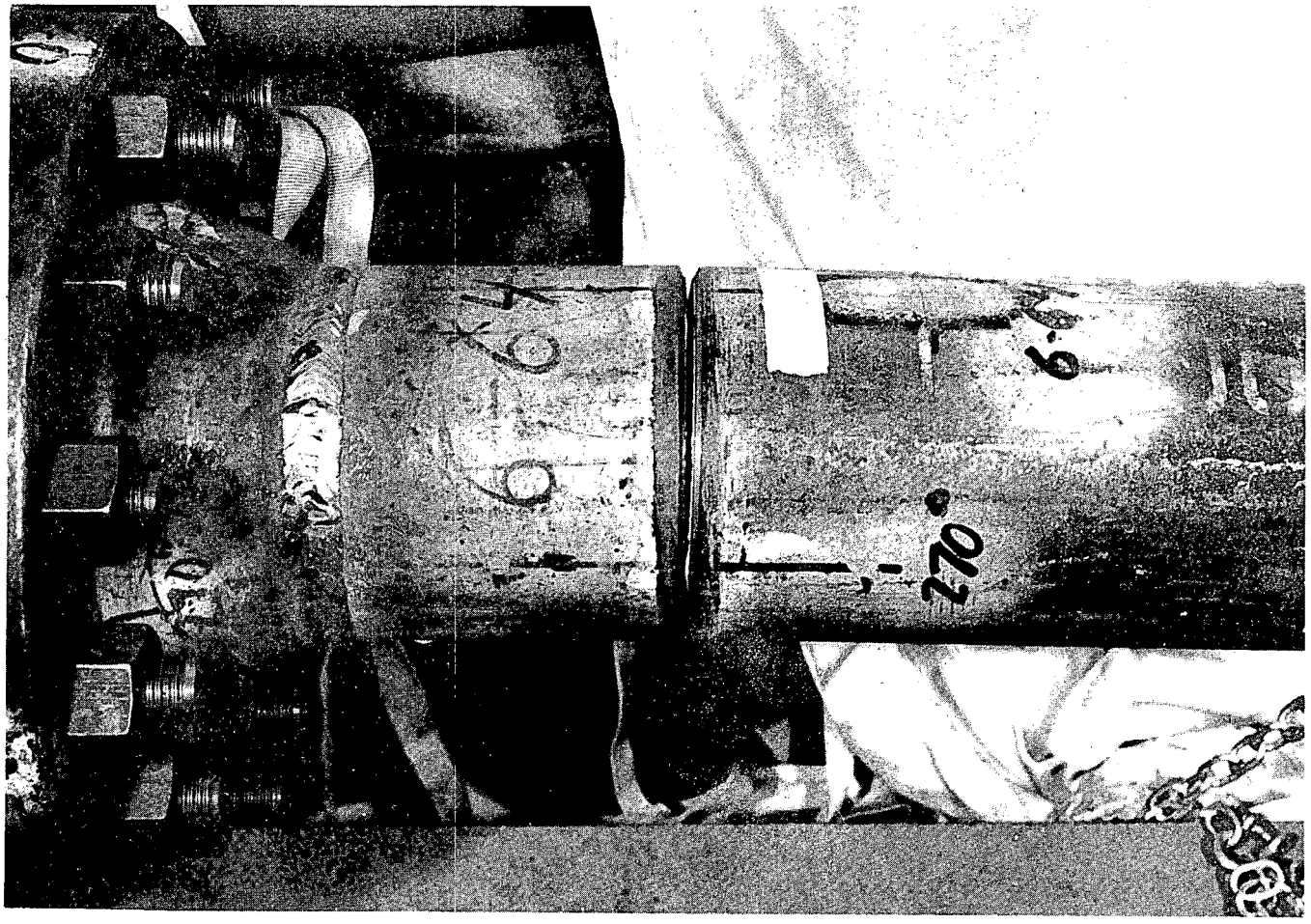

Figure 13. Pipe with Circumferential Part-Through Flaw, Bending Only

Table 4
PIPE FITTING TEST DATA

Specimen No.	Type	Flaw Type[a]	Maximum Flaw Length (inches)	Burst Pressure (ksi)	Average Flaw Length (inches)	P/P_o	x/T	$T_{,av}$
EL-1-8	Ell	none	0	8.68	0	1.00	1.00	0.453
EL-1A-8	Ell	A	3.25	6.56	3.1	0.76	0.39	0.490
EL-2A-8	Ell	A	6.41	4.70	6.3	0.54	0.30	0.463
EL-3A-8	Ell	A	6.31	6.47	6.2	0.74	0.63	0.444
EL-1B-8	Ell	B	8.25	5.86	7.5	0.67	0.29	0.443
EL-2B-8	Ell	B	11.59	6.09	10.7	0.70	0.51	0.447
EL-1C-8	Ell	C	8.66	5.21	7.9	0.60	0.35	0.471
EL-2C-8	Ell	C	7.94	7.05	7.2	0.81	0.63	0.445
EL-3C-8	Ell	C	5.69	4.70	4.9	0.54	0.28	0.423
T-1-8	Tee	none	0	8.88	0	1.00	1.00	0.655
T-1J-8	Tee	J	5.69	6.33	5.0	0.71	0.78	0.645
T-2J-8	Tee	J	4.25	6.98	3.0	0.79	0.45	0.622
T-3J-8	Tee	J	6.25	5.84	5.2	0.66	0.45	0.638
T-1K-8	Tee	K	1.95	6.30	1.7	0.71	0.73	0.612
T-2K-8	Tee	K	1.75	6.70	1.0	0.75	0.70	0.641
T-3K-8	Tee	K	2.45	4.88	1.3	0.55	0.43	0.559
T-1L-8	Tee	L	5.5	8.85	4.7	1.00-	0.77	0.646
T-2L-8	Tee	L	6.0	9.00	5.0	1.00	0.55	0.645
T-3L-8	Tee	L	4.0	9.18	29	1.00	0.43	0.685

[a] *See Figure 2*

Figure 14. Fracture Appearance in Tee Tested to Failure

Figure 15. Gross Failure Appearance, Unflawed Elbow

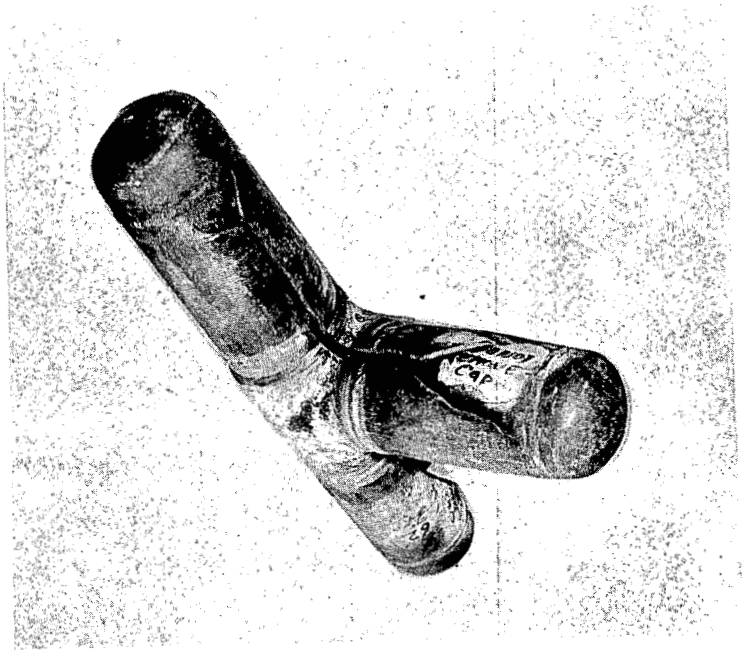

Figure 16. Gross Failure Appearance, Unflawed Tee

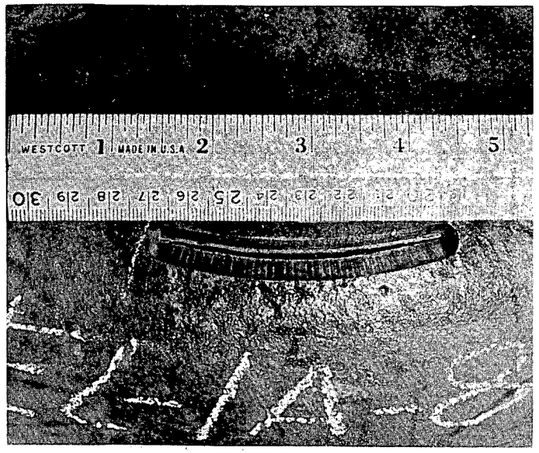

EL-1A-8

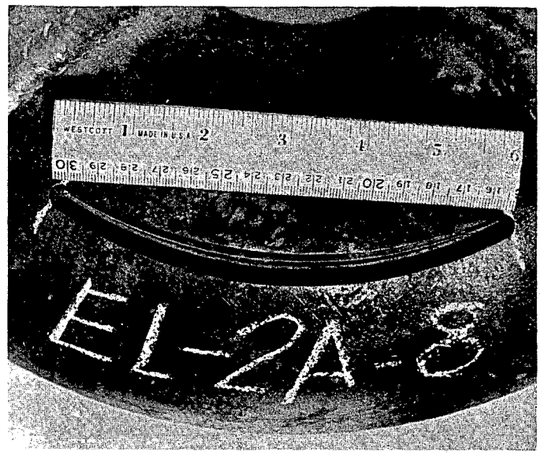

EL-2A-8

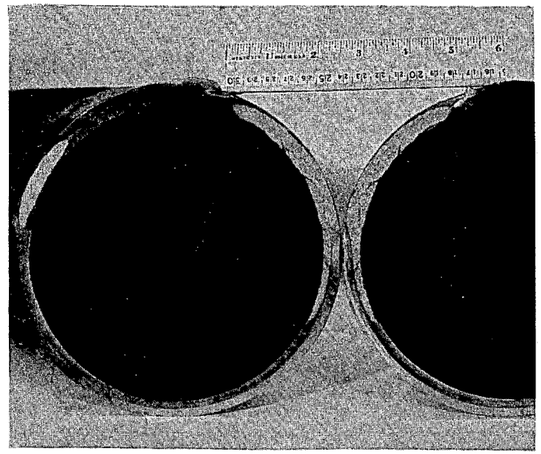

EL-2B-8

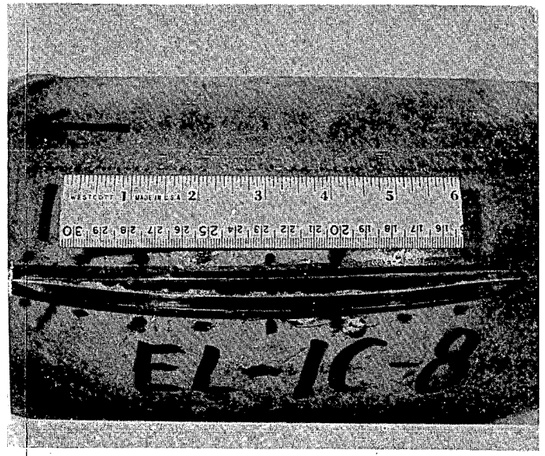

EL-1C-8

EL-3A-8

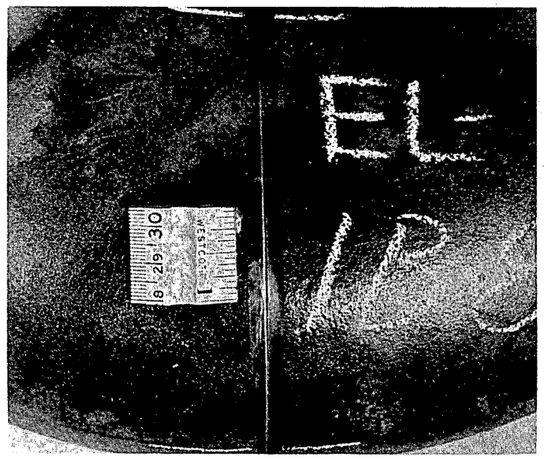

EL-1B-8

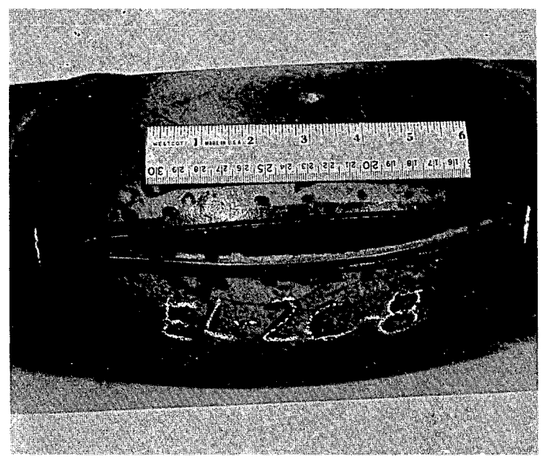

EL-2C-8

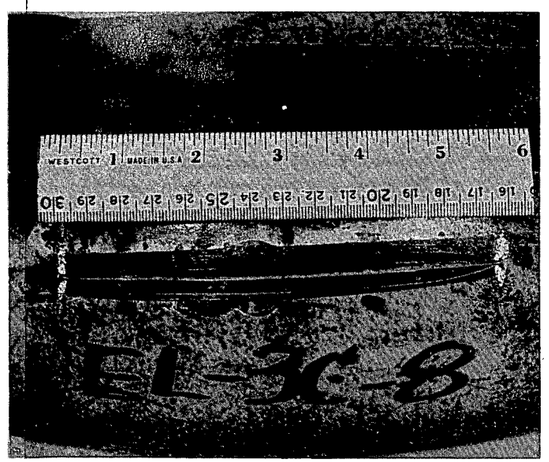

EL-3C-8

SEE TABLE 5-1

Figure 17. Failure Appearances, Flawed Elbows

T–1J–8

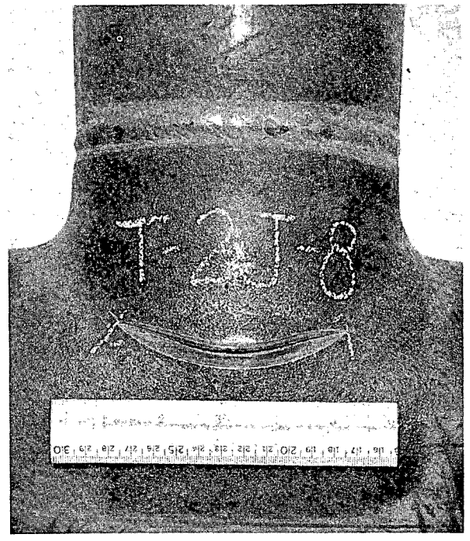

T–2J–8

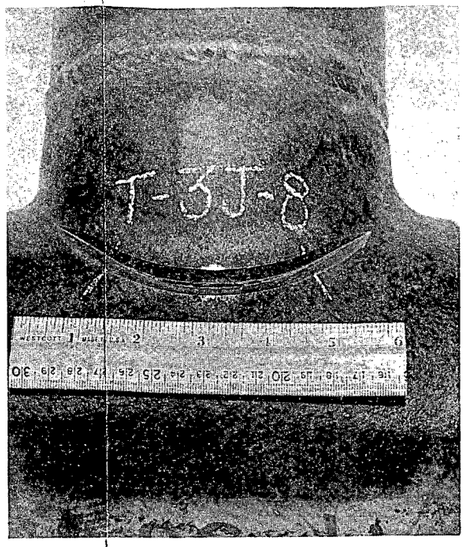

T–3J–8

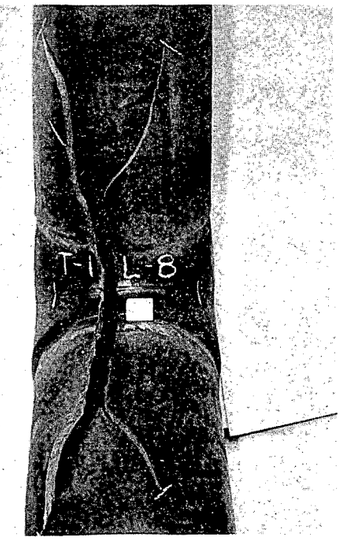

T–1L–8

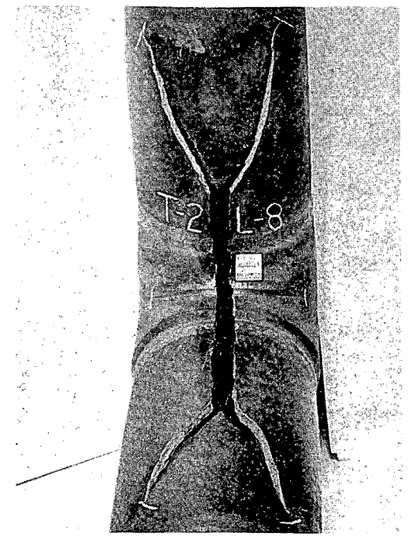

T–2L–8

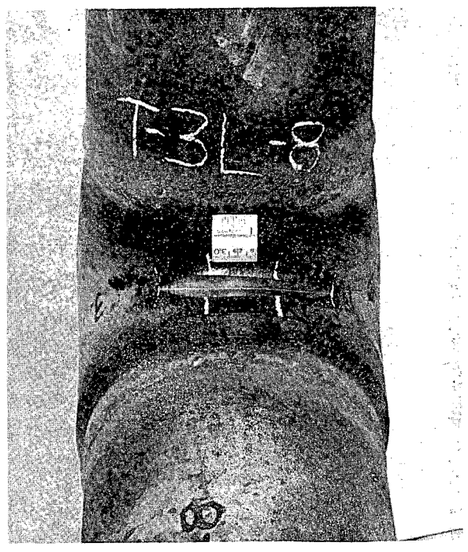

T–3L–8

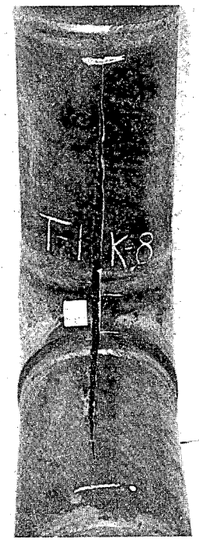

T–1K–8

T–2K–8

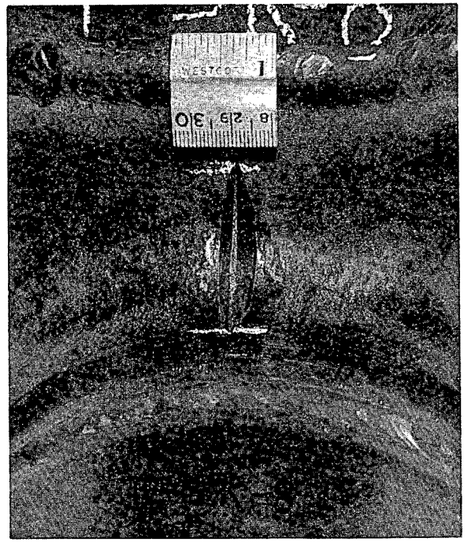

T–3K–8

SEE TABLE 5–1

Figure 18. Failure Appearances, Flawed Tees

5. SUMMARY

It has been found that while the instability behavior of carbon steel pipes containing axial through-wall flaws cannot be predicted accurately by unmodified linear elastic fracture mechanics relationships, it is not difficult to arrive at empirical expressions which predict the failure of such pipes with acceptable accuracy, at least for ASTM A106B pipe at 60°F in sizes from 4-to-12-inch nominal diameter.

Pressure load limit data for pipes containing short, part-through axial flaws are presented in the form of a "failure diagram," in which burst pressure relative to the unflawed condition is plotted against the reciprocal of flaw length. From such a diagram the approximate burst strength for a pipe with a flaw of any given length and depth can be estimated.

"Axial" (i.e., parallel to flow lines) part-through flaws in elbows were found to behave much as axial part-through flaws in pipes if differences in circumferential to axial stress ratios were accounted for in the comparison. No exact analysis was attempted in the case of flawed tees, but in-place flaws in the crotch of a tee or axial flaws in the side of a tee were found to cause marked reductions in strength.

REFERENCES

1. *Reactor Primary Coolant System Rupture Study, Quarterly Progress Report No. 10, July–September 1967,* December 1967, (GEAP-5554), p. 34.
2. Irwin, G. R., "Fracture," *Handbuch der Physik,* Springer-Verlag, Berlin, 1958, Vol. 6, pp. 551-590.
3. Anderson, R. B., *Fracture Mechanics of Through-Cracked Cylindrical Pressure Vessels,* American Society for Metals, Metals Park, Ohio, 1965 (Technical Report No. W4-4-65).
4. Irvine, W. H., Quirk, A., and Bevitt, E., *Fast Fracture of Pressure Vessels: An Appraisal of Theoretical and Experimental Aspects and Application to Operational Safety,* J. Brit. Nucl. Energy Soc., January 1964, p. 31.
5. Eiber, R. J., Hein, A. M., Duffy, A. R., and Atterbury, T J., *Investigation of the Initiation and Extent of Ductile Pipe Rupture,* Battelle Memorial Institute, Columbus, Ohio, January 1967 (BMI-1793).
6. Folias, E. S., "An Axial Crack in a Pressurized Cylindrical Shell," *Int. J. Fracture Mechanics,* **1**, 104 (1965).
7. Eiber, R. J., Hein, A. M., Duffy, A. R., and Atterbury, T J., *Investigation of the Initiation and Extent of Ductile Pipe Rupture,* Battelle Memorial Institute, Columbus, Ohio, November 1968 (BMI-1853).
8. Harris, D. O., *Stress Intensity Factors for Hollow Circumferentially Notched Round Bars,* Lawrence Radiation Laboratory, University of California, Livermore, Calif., April 1966, (UCRL-14859).
9. Gilman, J. D., *Stress Intensity Factor for a Circumferential Through-Wall Crack in a Straight Pipe,* January 1968, (GEAP-5557).
10. Folias, E. S., *On the Prediction of Failure in Pressurized Vessels,* College of Engineering, University of Utah, Salt Lake City, Utah, January 1969, (Report UTEC-CE-006).

ACKNOWLEDGMENT

The writer extends his appreciation to G. H. Henderson, who conducted the experimental tests.

DISTRIBUTION

Aerojet General
Engineering Division
Sacramento Plant
Sacramento, California 95801
Attn. Dr. F.J. Climent — 1

Advisory Committee on Reactor Safeguards
Dr. Spencer H. Bush
Consultant to the Director
Battelle Memorial Institute
Pacific Northwest Laboratory
Richland, Washington 99352 — 1

Advisory Committee on Reactor Safeguards
Mr. Harold Etherington
84 Lighthouse Drive
Jupiter, Florida 33458 — 1

Advisory Committee on Reactor Safeguards
Dr. William L. Faith
2540 Huntington Drive
San Marino, California 91108 — 1

Advisory Committee on Reactor Safeguards
Dr. Chester P. Siess
Department of Civil Engineering
3129 Civil Engineering Bldg.
University of Illinois
Urbana, Illinois 61801 — 1

Advisory Committee on Reactor Safeguards
Dr. Stephen H. Hanauer
Professor of Nuclear Engineering
606 Dougherty Hall
University of Tennessee
Knoxville, Tennessee 37916 — 1

Advisory Committee on Reactor Safeguards
Dr. Joseph M. Hendrie
Nuclear Engineering Department
Brookhaven National Laboratory
Upton, New York 11973 — 1

Advisory Committee on Reactor Safeguards
Dr. Herbert S. Isbin
Department of Chemical Engineering
University of Minnesota
Minneapolis, Minnesota 55455 — 1

Advisory Committee on Reactor Safeguards
Dr. Harry O. Monson, Senior Engineer
Laboratory Director's Office
Argonne National Laboratory
9700 South Cass Avenue
Argonne, Illinois 60439 — 1

Advisory Committee on Reactor Safeguards
Dr. Arlie A. O'Kelly
2421 West Rowland Avenue
Littleton, Colorado 80120 — 1

Advisory Committee on Reactor Safeguards
Dr. David Okrent, Senior Physicist
Laboratory Director's Office
Argonne National Laboratory
9700 South Cass Avenue
Argonne, Illinois 60439 — 1

Advisory Committee on Reactor Safeguards
Dean Nunzio J. Palladino
College of Engineering
The Pennsylvania State University
101 Hammond Building
University Park, Pennsylvania 16802 — 1

Advisory Committee on Reactor Safeguards
Dr. William R. Stratton
Los Alamos Scientific Laboratory
P. O. Box 1663
Los Alamos, New Mexico 87544 — 1

Advisory Committee on Reactor Safeguards
Dr. Carroll W. Zabel
Director of Research
University of Houston
Cullen Boulevard
Houston, Texas 77004 — 1

Mr. Raymond F. Fraley
Executive Secretary
Advisory Committee on Reactor Safeguards
U.S. Atomic Energy Commission
Room 1034-H
Washington, D.C. 20545 — 3

Argonne National Laboratory
9700 South Cass Avenue
Argonne, Illinois
Attn: Mr. Paul G. Shewmon — 1

Argonne National Laboratory
9700 South Cass Avenue
Argonne, Illinois
Attn: Dr. P. Lottes — 1

Argonne National Laboratory
9700 South Cass Avenue
Argonne, Illinois
Attn: Dr. C.E. Dickerman — 1

Argonne National Laboratory
9700 South Cass Avenue
Argonne, Illinois
Attn: Dr. R.O. Ivins — 1

Argonne National Laboratory
9700 South Cass Avenue
Argonne, Illinois
Attn: Dr. S. Fistedis — 1

Argonne National Laboratory
9700 South Cass Avenue
Argonne, Illinois
Attn: Dr. R.C. Vogel — 1

Argonne National Laboratory
9700 South Cass Avenue
Argonne, Illinois
Attn: LMFBR Program Office — 1

Argonne National Laboratory
9700 South Cass Avenue
Argonne, Illinois
Attn: Mr. A. Amorosi — 2

Argonne National Laboratory
9700 South Cass Avenue
Argonne, Illinois
Attn: Dr. L. Baker — 1

Atomic Energy Commission
Division of Reactor Development and Technology
Washington, D.C. 20545
Attn: Col. R.L. Ednie
Asst. Director for Army Reactors — 1

Atomic Energy Commission
Division of Reactor Development and Technology
Washington, D.C. 20545
Attn: Mr. M.A. Rosen
Asst. Director for Plant Engineering — 1

Advisory Committee on Reactor Safeguards
Mr. Harold G. Mangelsdorf
78 Knollwood Road
Short Hills, New Jersey 07078 — 1

Atomic Energy Commission
Division of Reactor Development and Technology
Washington, D.C. 20545
Attn: Mr. M.J. Whitman
Asst. Director for Program Analysis — 1

Atomic Energy Commission
Division of Reactor Development and Technology
Washington, D.C. 20545
Attn: Dr. E.E. Sinclair
Asst. Director for Reactor Technology — 1

Atomic Energy Commission
Division of Reactor Development and Technology
Washington, D.C. 20545
Attn: Mr. A. Giambusso
Asst. Director for Project Management — 1

Atomic Energy Commission
Division of Reactor Development and Technology
Washington, D.C. 20545
Attn: Mr. E.E. Kintner
Asst. Director for Reactor Engineering — 1

Atomic Energy Commission
Division of Reactor Development and Technology
Washington, D.C. 20545
Attn: Mr. J. W. Crawford
Asst. Director for Engineering Standards — 1

Atomic Energy Commission
Division of Compliance, Region IV
10395 West Colfax Avenue
Denver, Colorado 80215
Attn: Mr. John W. Flora — 1

Atomic Energy Commission
Division of Compliance
Washington, D.C. 20545
Attn: Mr. L. Kornblith, Jr. — 1

Atomic Energy Commission
Division of Operational Safety
Washington, D.C. 20545
Attn: Mr. H. Gilbert — 1

Atomic Energy Commission
Division of Reactor Standards
Washington, D.C. 20545
Attn: Mr. E.G. Case — 10

Atomic Energy Commission
Division of Reactor Standards
Washington, D.C. 20545
Attn: Mr. M. Bolotsky — 1

Atomic Energy Commission
Division of Reactor Standards
Washington, D.C. 20545
Attn: Mr. A.B. Holt — 1

Atomic Energy Commission
Division of Reactor Standards
Washington, D.C. 20545
Attn: Mr. R. Waterfield — 1

Atomic Energy Commission
Division of Reactor Standards
Washington, D.C. 20545
Attn: Dr. G. Burley — 1

Atomic Energy Commission
Division of Reactor Standards
Washington, D.C. 20545
Attn: Mr. R. Impara — 1

Atomic Energy Commission
Water Projects Branch
Division of Reactor Development and Technology
Washington, D.C. 20545
Attn: Mr. W.H. Layman — 1

Atomic Energy Commission
Naval Reactors Branch
Division of Reactor Development and Technology
Washington, D.C. 20545
Attn: Mr. R.S. Brodsky — 2

Atomic Energy Commission
Division of Reactor Development and Technology
Washington, D.C. 20545
Attn: A.J. Pressesky — 7

Atomic Energy Commission
Division of Reactor Development and Technology
Washington, D.C. 20545
Attn: Mr. S.A. Szawlewicz — 5

Atomic Energy Commission
Division of Reactor Development and Technology
Washington, D.C. 20545
Attn: Mr. R.R. Newton — 1

Atomic Energy Commission
Division of Production
Washington, D.C. 20545
Attn: Mr. George B. Pleat — 1

Atomic Energy Commission
c/o Gulf General Atomic, Inc.
P.O. Box 608
San Diego, California 92112
Attn: Mr. Russell H. Ball — 1

Atomics International
P.O. Box 309
Canoga Park, California
Attn: Dr. H. Morewitz — 2

Babcock & Wilcox Company
Washington Operations Office
1725 I Street, N.W.
Washington,D.C. 20006 — 1

Babcock & Wilcox Company
P.O. Box 1260
Lynchburg, Virginia
Attn: Mr. Robert Wascher — 1

Battelle Memorial Institute
505 King Avenue
Columbus, Ohio 43201
Attn: Dr. D.N. Sunderman — 2

Battelle Memorial Institute
505 King Avenue
Columbus, Ohio 43201
Attn: Dr. D.L. Morrison — 1

Battelle Memorial Institute
505 King Avenue
Columbus, Ohio 43201
Attn: Mr. S. Paprocki — 2

Battelle Memorial Institute
505 King Avenue
Columbus, Ohio 43201
Attn: Mr. A.R. Duffy — 1

Brookhaven National Laboratory
Upton, Long Island, New York 11973
Attn: A.W. Castleman — 1

University of California
Institute of Engineering Research
Berkeley, California 94704
Attn: Prof. V.E. Schrock — 1

Hans A. Maurer
Commission of the European Communities
Rue De La L01 200
1040 Brussels, Belgium — 1

Canoga Park Area Office
P.O. Box 591
Canoga Park, California 91305
Attn: Mr. R.L. Morgan RDT Senior Site Rep. — 1

Combustion Engineering, Inc.
Nuclear Division
P.O. Box 500
Windsor, Connecticut 06095
Attn: Mr. M.F. Valerino — 1

Chicago Operations Office
Atomic Energy Commission
9800 South Cass Avenue
Argonne, Illinois 60439
Attn: Mr. D.M. Gardiner — 1

Douglas United Nuclear
Richland, Washington
Attn: Mr. John Riches — 1

Harvard Air Cleaning Laboratory
Harvard University
665 Huntington Avenue
Boston, Massachusetts 02190 — 1

IIT Research Institute
10 W. 35th Street
Chicago, Illinois 60616
Attn: Dr. T.A. Zaker — 1

IIT Research Institute
10 W. 35th Street
Chicago, Illinois 60616
Attn: Mr. E.V. Gallagher — 1

Idaho Operations Office
Atomic Energy Commission
P.O. Box 2108
Idaho Falls, Idaho 83401
Attn: Mr. D. Williams — 2

Liquid Metal Engineering Center
c/o Atomics International
P.O. Box 309
Canoga Park, California 91304
Attn: R.W. Dickinson — 1

Los Alamos Scientific Laboratory
P.O. Box 1663
Los Alamos, New Mexico 87544
Attn: Mr. J.H. Russel, K Division — 1

MPR Associates, Inc.
1140 Connecticut Avenue, N.W.
Washington, D.C. 20036
Attn: Mr. T. Rockwell III
Chairman AIF Safety Task Force — 1

National Bureau of Standards
Washington, D.C. 20545
Attn: Dr. C. Muehlhause — 1

Naval Ordnance Laboratory
White Oak
Silver Spring, Maryland
Attn: Mr. James Proctor — 1

North Carolina State University
Department of Mechanical Engineering
Raleigh, North Carolina 27607
Attn: Prof. M.N. Ozisik — 1

Nuclear Fuels Services
West Valley, New York 14171 — 1

Oak Ridge Operations Office
Atomic Energy Commission
Oak Ridge, Tennessee 37830
Attn: Mr. W.L. Smalley — 1

Oak Ridge National Laboratory
Nuclear Safety Information Center
P.O. Box Y
Oak Ridge, Tennessee 37830
Attn: Mr. Joel Buchanan — 1

Chemical Technology Division
Oak Ridge National Laboratory
P.O. Box Y
Oak Ridge, Tennessee 37830
Attn: Mr. D. Ferguson — 1

Chemical Technology Division
Oak Ridge National Laboratory
P.O. Box Y
Oak Ridge, Tennessee 37830
Attn: Mr. R. Blanco — 1

Oak Ridge National Laboratory
P.O. Box Y
Oak Ridge, Tennessee
Attn: HTGR Safety Program Office — 2

Oak Ridge National Laboratory
P.O. Box Y
Oak Ridge, Tennessee
Attn: Mr. W. B. Cottrell — 4

Oak Ridge National Laboratory — 1
P.O. Box Y
Oak Ridge, Tennessee
Attn: Mr. P. Rittenhouse

Pacific Northwest Laboratories — 1
P.O. Box 999
Richland, Washington 99352
Attn: Mr. G. Rogers

Pacific Northwest Laboratories — 1
P.O. Box 999
Richland, Washington 99352
Attn: Mr. J.C. Spanner

Pacific Northwest Laboratories — 1
P.O. Box 999
Richland, Washington 99352
Attn: Dr. J. Batch

Pacific Northwest Laboratories — 2
P.O. Box 999
Richland, Washington 99352
Attn: Mr. R. Nightingale

Pacific Northwest Laboratories — 1
P.O. Box 999
Richland, Washington 99352
Attn: Mr. L. Schwendiman

Pacific Northwest Laboratories — 1
P.O. Box 999
Richland, Washington 99352
Attn: Mr. E.R. Astley, Mgr. FFTF

Idaho Nuclear Corporation — 1
P.O. Box 1845
Idaho Falls, Idaho 83401
Attn: Mr. Curt Haire

Idaho Nuclear Corporation — 2
P. O. Box 1845
Idaho Falls, Idaho 83401
Attn: Mr. S. O. Johnson

Idaho Nuclear Corporation — 2
P.O. Box 1845
Idaho Falls, Idaho 83401
Attn: Mr. H. L. Coplen

Idaho Nuclear Corporation — 1
P. O. Box 1845
Idaho Falls, Idaho 83401
Attn: Mr. O. F. Brockett

Idaho Nuclear Corporation — 3
P. O. Box 1845
Idaho Falls, Idaho 83401
Attn: Water Reactor Safety Program
Office, Mr. G. O. Bright, Mgr.

Richland Operations Office — 1
P.O. Box 500
Richland, Washington 99352
Attn: Mr. C. Robinson

Richland Operations Office — 1
P.O. Box 500
Richland, Washington 99352
Attn: Mr. A.S. Waterhouse

Richland Operations Office — 1
P.O. Box 500
Richland, Washington 99352
Attn: Mr. A. Brunstad

San Francisco Operations Office — 1
Atomic Energy Commission
2111 Bancroft Way
Berkeley, California 94704
Attn: Mr. C.V. Backlund

Savannah River Laboratories — 1
E.I. duPont deNemours and Company
Aiken, South Carolina 29802
Attn: Mr. A.H. Peters

TRW Inc. — 1
TRW Systems Group
One Space Park
Redondo Beach, California 90278
Attn: Dr. D. B. Langmuir

TRW Inc. — 1
TRW Systems Group
One Space Park
Redondo Beach, California 90278
Attn: Mr. S.M. Zivi

Westinghouse Electric Corporation — 1
Atomic Power Division
P.O. Box 355
Pittsburgh, Pennsylvania 15230
Attn: Mr. R.A. Wiesemann

Westinghouse Electric Corporation — 1
Atomic Power Division
P.O. Box 355
Pittsburgh, Pennsylvania 15230
Attn: Dr. D. Fletcher

Westinghouse Electric Corporation
Atomic Power Division
P.O. Box 355
Pittsburgh, Pennsylvania 15230
Attn: Dr. E. Beckjord

Westinghouse Electric Corporation
P.O. Box 19218
Tampa, Florida 33616
Attn: Mr. A. Lohmeier

Southern Nuclear Engineering, Inc.
P.O. Box 10
Dunedin, Florida 33528
Attn: Mr. Gilbert Brown

Holmes & Narver, Inc.
828 South Figueroa St.
Los Angeles, California 90017
Attn: B. Shimizu

Mr. Edward T. Wessel
Research and Development Center
Westinghouse Electric Corporation
Beulah Road, Churchill Boro
Pittsburgh, Pennsylvania 15235

Dr. William E. Cooper
Teledyne Materials Research
303 Bear Hill Road
Waltham, Massachusetts

Roger W. Staehle
Metallurgy Department
Ohio State University
Columbus, Ohio

Mr. Ralph Jones
Division of Reactor Development
U.S. Atomic Energy Commission
Washington 25, D.C.

Mr. H.K. Marks
Room 2N83
Department of the Navy
Washington, D.C.

H. Thielsch
140 Shaw Avenue
Cranston 5, Rhode Island

Knolls Atomic Power Laboratory
P. O. Box 1072
Schenectady, New York 12301
Attn: Dr. Robert A. Barnes

1

Mr. F.M. Moschine
Westinghouse Electric Company
Atomic Power Department
P.O. Box 355
Pittsburgh, Pennsylvania 15230

1

Dr. P. L. Pfenningwerth
Bettis Atomic Power Laboratory
P.O. Box 79
West Mifflin, Pennsylvania 15122

1

Professor C.E. Taylor
Department of Theoretical and Applied Mechanics
University of Illinois
Urbana, Illinois

1

Mr. E. Beauchamp-Nobbs
U.S. Marine Engineering Laboratory
Annapolis, Maryland

3

U.S. Atomic Energy Commission
1 Division of Technical Information Extension
P.O. Box 62
Oak Ridge, Tennessee

1

U.S. Atomic Energy Commission
Division of Reactor Licensing
1 Washington, D.C. 20545
Attn: S.S. Pawlicki

1

USAEC Site Representative
General Electric Company
1 Sunnyvale, California 94086
Attn: Joel Levy, Senior Site Rep.

1

Mr. B.L. Greenstreet
P.O. Box Y
1 Oak Ridge National Laboratory
Oak Ridge, Tennessee

1

Mr. F.J. Witt
P.O. Box Y
1 ORNL - Oak Ridge, Tennessee

2

Commonwealth Edison Company
Dresden Nuclear Power Station
Rural Route 1
1 Morris, Illinois 60450
Attn: H.K. Hoyt

3

Commonwealth Edison Company
1 System Mechanical and Structural Engineer
72 West Adams Street
Chicago, Illinois 60690
Attn: N.A. Kershaw

United Kingdom Atomic Energy Authority
Reactor Materials Laboratory
Wigshaw Lane, Culcheth
Warrington, Lancs.
England
Attn: R.W. Nichols — 1

Atomic Energy of Canada Limited
Chalk River Nuclear Laboratories
Chalk River, Ontario, Canada
Dr. George Pon — 1

Mr. Robert D. Wylie
Department of Materials Engineering
Southwest Research Institute
8599 Culebra Road
San Antonio, Texas 78228 — 1

O.A. Kellerman
Institut Fur Reaktorsicherheit
Der Technischen Uberwachungs
Vereine, e.V.
5 KOLN 1 Glockengasse 2
West Germany — 1

C. A. G. Phillips
U.K.A.E.A. Safeguards Division
Authority Health & Safety Branch
Risley, Warrington, Lancashire
England — 1

Division of Reactor Development & Technology
U.S. Atomic Energy Commission
Washington, D.C. 20545
Attn: J. R. Hunter — 1

Mr. T. R. Magee
Westinghouse Electric Co.
PWR Systems Division
P.O. Box 355
Pittsburgh, Pennsylvania 15230 — 1

Reactor Materials Branch
Metallurgy Division
Naval Research Laboratory
Washington, D. C. 20545
Attn: Mr. L. E. Steele — 1

Department of Material Science & Engineering
Hearst Mining Building
University of California
Berkeley, California
Attn: Mr. William W. Gerberich — 1

United Engineers and Constructors, Inc.
1401 Arch Street
Philadelphia, Pennsylvania 19105
Attn: Mr. John Crowley — 1

Argonne National Laboratory
9700 South Cass Avenue
Argonne, Illinois
Attn: Mr. Craig Cheng — 1

AEG Telefunken
AEC Hochhaus Sued
6 Frankfurt/Main 70
West Germany
Attn: Mr. Dieter Ewers — 1

Asst. Director, Instruction Division
U.S. Atomic Energy Commission
Chicago Operations Office
9800 South Cass Avenue
Argonne, Illinois 60439
Attn: R. M. Moser — 1